Achary, S.N.; Errandonea, D.; Muñoz, A.; Rodríguez Hernández, P.;Manjón, F.J.; Kishna, P. S. R.; Patwe, S. J.; Grover, V. ; Tyagi, A. (2013). Experimental and theoretical investigations on the polymorphism and metastability of BiPO4. Dalton Transactions. 42:14999-15015. doi:10.1039/c3dt51823j.

Experimental and theoretical investigations on polymorphism and metastability of $BiPO_4$

S. N. Achary[1*], D. Errandonea [2], A. Muñoz[3], P. Rodríguez-Hernández[3], F. J. Manjón[4], P. S. R. Krishna [5], S. J. Patwe[1], V. Grover[1] and A. K. Tyagi [1]

[1]Chemistry Division, Bhabha Atomic Research Centre, Mumbai 400085, India
[2]MALTA Consolider Team, Departamento de Física Aplicada-ICMUV, Universitad de Valencia, Edificio de Investigación, c/Dr. Moliner 50, Burjassot, 46100 Valencia, Spain
[3]Departamento de Física Fundamental II, Instituto de Materiales y Nanotecnología, MALTA Consolider Team, Universidad de La Laguna, La Laguna 38205, Tenerife, Spain
[4] Instituto de Diseño para la Fabricación y Producción Automatizada, MALTA Consolider Team, Universitat Politècnica de València, 46022 València, Spain
[5]Solid State Physics Division, Bhabha Atomic Research Centre, Mumbai 400085, India

Abstract

In this communication we report the metastabilty and energetic of phase transitions of three different polymorphs of $BiPO_4$, namely trigonal (Phase-I, space group $P3_121$), monoclinic monazite-type (Phase-II, space group $P2_1/n$) and $SbPO_4$-type monoclinic (Phase-III, space group $P2_1/m$) from ambient and non ambient temperature powder XRD and neutron diffraction studies as well as *ab initio* Density Functional Theory (DFT) calculations. The symmetry ambiguity between $P2_1$ and $P2_1/m$ of the high temperature polymorph of $BiPO_4$ has been resolved by neutron diffraction study. The structure and vibrational properties of these polymorphs of the three polymorphs have also been reported in detail. The total energy calculations have been used to understand the experimentally observed metastable behavior of trigonal and monazite-type $BiPO_4$. Interestingly, all the three phases were found to coexist after heating a single phasic trigonal $BiPO_4$ to 773 K. The irreversible natures of these phase transitions have been explained on the concepts of interplay of structural distortion, molar volume and total energy.

Address for Correspondence
Dr. S. N. Achary,
Chemistry Division, Bhabha Atomic Research Centre, Mumbai – 400 085, India
Email: sachary@barc.gov.in; acharysn@rediffmail.com
Phone: 0091-22-2559 2328; Fax : 0091-22-2550 5151

Lattice-dynamic calculations of the phonon modes were performed at the zone center (Γ point) of the BZ. We used a direct force-constant approach (or supercell method) [43] as it is conceptually simple. These calculations provide information about the symmetry of the modes and their polarization vectors which allowed us to identify the irreducible representations and the character of the phonon modes at the Γ point. However, this method did not include the contribution from dipole-dipole interactions resulting the LO-TO splitting of infrared-active modes, due to the non-analyticity of this term at the Γ point.

4. Results and discussion

4.1. X-ray and neutron diffraction studies at ambient conditions

The powder XRD patterns of the three phases of $BiPO_4$, namely BiPO4-I, II and III (shown in Fig. 1) are in agreement with trigonal, monoclinic monazite-type (JCPDS-PDF-80-0209) and monoclinic high-temperature $SbPO_4$ type (JCPDS-PDF-77-2208), respectively. The complete transformation from one phase to other and retention of the transformed phases is a unique example observed in $BiPO_4$ compared to other orthophosphates of trivalent cations. It has been argued that that the water molecules in $BiPO_4$ play a crucial role in stabilizing the trigonal structure of $BiPO_4$-I. [32] Such hydrated hexagonal forms have been reported for almost all the trivalent rare-earth cations and upon dehydration the structure is destabilized and transforms to other structure types. [44] The comparable coherent neutron scattering lengths of various atoms and negative scattering length of the hydrogen ($b_O = 0.580 \times 10^{-12}$ cm, $b_{Bi} = 0.853 \times 10^{-12}$ cm, $b_P = 0.513 \times 10^{-12}$ cm, $b_H = -0.374 \times 10^{-12}$ cm) were helpful to obtain accurate structural parameters by neutron diffraction compared to the x-ray diffraction. The detailed structural parameters of the three phases were obtained by Rietveld refinement of the powder neutron diffraction data. The initial structural models for the for the Rietveld refinements were taken from the structural data reported by Romero et al. [32] (for trigonal $BiPO_4$-I and monazite-type $BiPO_4$-II) and Masse and Duriff [31] (for high-temperature $BiPO_4$-III). Diffractometer zero and sample displacements parameters were taken from the neutron diffraction pattern of standard Yb_2O_3. The peaks of the neutron diffraction patterns were computed by using Pseudo-Voigt profile function. The backgrounds of the patterns were fitted with shifted Chebyschev polynomial functions. It can be

evident. This observation is supported by first principle total energy calculations explained later in this manuscript. The different trends in variation of unit cell parameters of $BiPO_4$-I are reflected in the variation of unit cell volume (**Fig. 7**). The variation of molar volume (V/Z) of $BiPO_4$-I with temperature shows feeble decreasing trend up to 473 K. This initial decreasing trend can be assigned to the contraction of the lattice due to the loss of water molecules from the hexagonal channel in the lattice. A subtle positive expansion behavior in between 473 and 673 K can be attributed thermal expansion behavior of anhydrous trigonal $BiPO_4$ (Phase-I). In a condition, the trigonal, monazite-type and $SbPO_4$-type phase can exist with stoichiometry as $BiPO_4$ and thus they can be regarded as polymorphic transition.

Detailed analyses of the refined structural parameters of the different polymorphs suggest that the PO_4 tetrahedra are regular in the monazite-type ($BiPO_4$-II) and $SbPO_4$-type ($BiPO_4$-III) phases compared to those the trigonal phase. The polyhedral characters of the three phases were calculated by IVTON [52, 53] and they are given in **Table 4**. It can be mentioned here that the PO_4 tetrahedra in trigonal phase do not act like a rigid unit as commonly observed in most phosphates. The average bond lengths of P-O of trigonal phase are also longer compared to other two phases. Similar analyses of coordination polyhedra around Bi in the three phases indicate that the BiO_8 or BiO_9 units of the $BiPO_4$ phases are distorted and asymmetric. Further the volume distortion [53] (relative difference between the volume of polyhedra and volume of ideal polyhedra expected for a same radius of circumscribed sphere) and eccentricity (deviation of central atom position from the ideal centre of the coordination polyhedron) of the BiO_n polyhedra are larger in trigonal phase compared to the other two phases. The details of polyhedral analyses of the high temperature structures are given in Electronic Supplementary Information (ESI-I) [†]. The larger eccentricity and asymmetry of the trigonal phase is minimized by the additional bonding interaction from the H_2O molecules in the lattice. It is observed that the average Bi-O bond lengths and distortion in BiO_8 polyhedra increase with the increase in temperature. The increasing trend is significant for trigonal (I) and monazite (II) type phases compared to the $SbPO_4$ type phase (III). This result suggests that the $SbPO_4$ type phase is the stable phase for $BiPO_4$ at ambient condition. The relatively expanded lattice can be attributed to the higher stability of $SbPO_4$-type phase. In the next section we further study the stability of these phases by means of *ab-initio* theoretical calculations.

5. Conclusions

In summary, the detailed analyses of the powder X-ray and neutron diffraction data as well as IR and Raman studies on three polymorphs of $BiPO_4$ revealed accurate structural parameters and local distortions parameters around $Bi^{3+}$and P^{5+}. Further the structural parameters and vibrational frequencies were supported by *ab initio* calculations based on DFT. The irreversible trigonal-monazite-$SbPO_4$-type structural transitions are explained from the molar volume and total energy of the three phases. Highly distorted structural arrangement around Bi^{3+} and P^{5+} has a very limited stability and is only stabilized by water molecules in the trigonal phase. It is revealed that structural transition from trigonal to monazite or $SbPO_4$ type structures is accompanied by a significant reduction in volume. DFT calculations revealed that the monazite and $SbPO_4$-type $BiPO_4$ have almost similar total energy and hence a competing stability. Further it is observed that monazite type phase shows larger lattice thermal expansion compared to the $SbPO_4$-type phase and thus it is truly a metastable phase.

Acknowledgements

This study was supported by the Spanish government MEC under Grants No: MAT2010-21270-C04-01/04, by MALTA Consolider Ingenio 2010 project (CSD2007-00045), and by the Vicerrectorado de Investigación y Desarrollo of the Universidad Politécnica de Valencia (UPV2011-0914 PAID-05-11 and UPV2011-0966 PAID-06-11). S.N.A. acknowledges the support provided by Universitat de Valencia during his visit to it. A.M. and P.R-H. acknowledge computing time provided by Red Española de Supercomputación (RES) and MALTA-Cluster.

†Electronic Supplementary Information (ESI) available: [(ESI-1). Further details of crystal structural data of the BiPO4-I, II and III can be obtained from the Fachinformationszentrum Karlsruhe, Abt. PROKA, 76344 Eggenstein-Leo-poldshafen, Germany (fax +49-7247-808-666; E-mail: crysdata@fiz-karlsruhe.de) on quoting the depository numbers CSD 426230 to 426255 (26 structures)]. See DOI: 10.1039/b000000x

Tables

Table 1: Refined unit cell parameters for different polymorphs of $BiPO_4$ at ambient temperature (300K). (Calculated unit cell parameters are also included for comparison)

Table-2: Refined and calculated structural parameters of $BiPO_4$ at 300K ((a). Trigonal (I), (b). Monazite-type (II) and (c). $SbPO_4$-type (III)).

Table 3: The typical bond lengths and polyhedral parameters in different phases of $BiPO_4$.

Table 4: Calculated and observed Infrared modes of different $BiPO_4$ phases. ((a). Trigonal (I), (b). Monazite-type (II) and (c). $SbPO_4$-type (III).)

Table 5: Calculated and observed Raman modes of $BiPO_4$ phases. ((a). Trigonal (I), (b). Monazite-type (II) and (c). $SbPO_4$-type (III)).

Table 3: The typical bond lengths and polyhedral parameters in different phases of $BiPO_4$.

$BIPO_4$-I (Trigonal)		$BIPO_4$-II (Monazite-type)		$BIPO_4$-III ($SbPO_4$-type)	
Bi - O1	2.817(8) (Å)	Bi - O1	2.580(6) (Å)	Bi - O1	2.149(4) (Å)
Bi - O1	2.296(8)	Bi - O1	2.492(5)	Bi - O1	2.880(4)
Bi - O1	2.817(7)	Bi - O2	3.020(5)	Bi - O2	2.896(4)
Bi - O1	2.296(12)	Bi - O2	2.399(6)	Bi - O2	2.330(3)
Bi - O2	2.378(7)	Bi - O2	2.700(5)	Bi - O3	2.357(3)
Bi1 -O2	2.490(9)	Bi - O3	2.361(6)	Bi - O3	2.526(3)
Bi - O2	2.490(7)	Bi - O3	2.394(6)	Bi - O3	2.526(3)
Bi - O2	2.378(8)	Bi - O4	2.469(5))	Bi - O3	2.357(3)
		Bi - O4	2.426(6)		
CN:	6+2	CN	8+1	CN	8
<Bi-O>	2.495(3) (Å)	$<Bi-O>_9$	2.538(2) (Å)	<Bi-O>	2.503(1) (Å)
Distt.	62.976 $x10^{-4}$	Distt.	60.598 $x10^{-4}$	Distt.	98.915 $x10^{-4}$
		$<Bi-O>_8$	2.478(2) (Å)		
		Distt.	18.238 $x10^{-4}$		
V_{BiO8} ($Å^3$)	29.06	V_{BiO8} ($Å^3$)	26.26	V_{BiO8} ($Å^3$)	27.28
Distt.	0.1491	Distt.	0.0684	Distt.	0.0819
Sphericity	0.844	Sphericity	0.941	Sphericity	0.910
Eccentricity	0.346	Eccentricity	0.196	Eccentricity	0.449
		V_{BiO9} ($Å^3$)	31.95		
		Distt.	0.0557		
		Sphericity	0.853		
		Eccentricity	0.308		
P – O1	1.523(12) (Å)	P - O1	1.550(7) (Å)	P - O1	1.554(4) (Å)
P - O1	1.523(9)	P - O2	1.567(7)	P - O2	1.552(4)
P - O2	1.592(9)	P - O3	1.539(6)	P - O3	1.526(3)
P - O2	1.592(10)	P -O4	1.509(8)	P - O3	1.526(3)
$<P-O>_4$	1.558(5) (Å)	$<P-O>_4$	1.541(4) (Å)	<P-O>	1.540(2) (Å)
Distt.	4.895 $x10^{-4}$	Distt.	1.839 $x10^{-4}$	Distt.	0.757 $x10^{-4}$
V_{PO4} ($Å^3$)	1.923	V_{PO4} ($Å^3$)	1.862	V_{PO4} ($Å^3$)	1.861
Distt.	0.0128	Distt.	0.0094	Distt.	0.0070
Sphericity	1	Sphericity	1	Sphericity	1
Eccentricity	0.042	Eccentricity	0.066	Eccentricity	0.116

(b). Monazite-type ($BiPO_4$-II)

Mode	LDA ω (cm^{-1})	Mode	PBESol ω (cm^{-1})	Mode	Exper ω (cm^{-1})
Ag(R)	64.378	Ag(R)	58.209	Ag	50,9
Ag(R)	74.285	Ag(R)	68.383	Ag	59,8
Bg(R)	75.286	Bg(R)	73.287	Bg	69,9
Bg(R)	93.699	Bg(R)	89.332	Bg	89,6
Ag(R)	97.335	Ag(R)	95.337	Ag	97,3
Bg(R)	106.908	Bg(R)	102.642	Bg	108,6
		Ag(R)	132.697	Bg	131,1
Bg(R)	134.561	Bg(R)	134.732	Bg	135,5
Ag(R)	138.597				
Ag(R)	166.950	Ag(R)	165.688	Ag	169,9
Bg(R)	172.921	Bg(R)	167.790	Bg + Ag	176,7
Ag(R)	172.787	Ag(R)	168.424		
Ag(R) + Bg(R)	192.601	Ag(R)	184.002	Ag + Bg	182,7
		Bg(R)	185.236		
Bg(R)	212.115	Bg(R)	203.883	Bg	207,4
Bg(R)	235.931	Bg(R)	226.199	Bg	229,8
Ag(R)	240.434	Ag(R)	231.903	Ag	237,1
Bg(R)	279.095	Bg(R)	271.332	Bg	272,5
Ag(R)	286.133	Ag(R)	278.671	Ag	283,5
Bg(R)	375.729	Bg(R)	368.303	Bg	388,4
Ag(R)	390.439	Ag(R)	384.549	Ag	407,4
Ag(R)	445.077	Ag(R)	438.688	Ag	457,0
Bg(R)	477.833	Bg(R)	469.945	Bg	463,5
Ag(R)	503.051	Ag(R)	497.999	Ag	495,9
Ag(R)	531.404	Ag(R)	527.220	Ag	522,7
Bg(R)	532.638	Bg(R)	527.287	Bg	557,1
Bg(R)	547.749	Bg(R)	540.930	Bg	572,6
Ag(R)	573.867	Ag(R)	568.083	Ag	598,3
Bg(R)	580.405	Bg(R)	573.921	Bg	604,5
Ag(R)	933.184	Ag(R)	911.936	Ag + Bg	926,3
Bg(R)	933.685	Bg(R)	915.772		
Ag(R)	954.933	Ag(R)	935.286	Ag	947,8
Ag(R)	973.412	Ag(R)	956.502	Ag	969,5
Bg(R)	982,552	Bg(R)	962.272	Bg	981,0
Bg(R)	1001.799	Bg(R)	985.256	Bg	1021,0
Ag(R)	1027.383	Ag(R)	1010.141	Ag	1039,4
Bg(R)	1035.389	Bg(R)	1016.612	Bg	1050,2

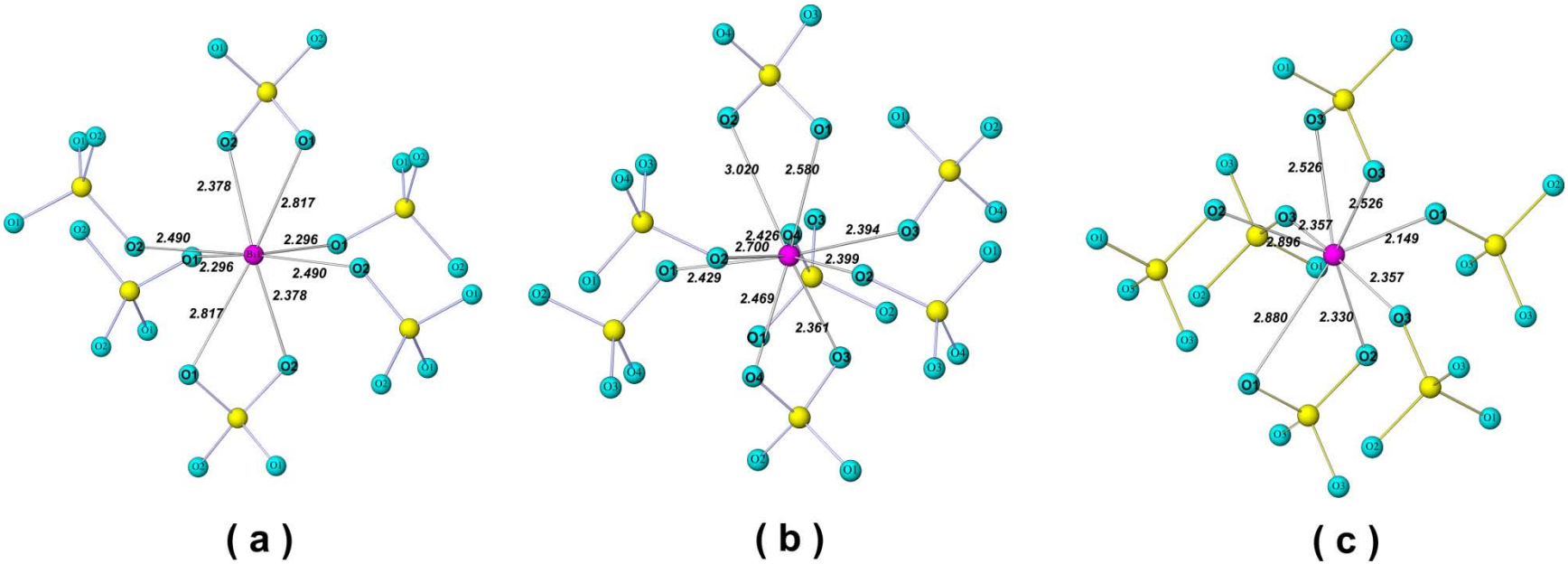

Fig. 4: Typical coordination around Bi^{3+} in $BiPO_4$ phases, (a). Trigonal (I), (b). Monazite type (II) and (c). $SbPO_4$ type (III)

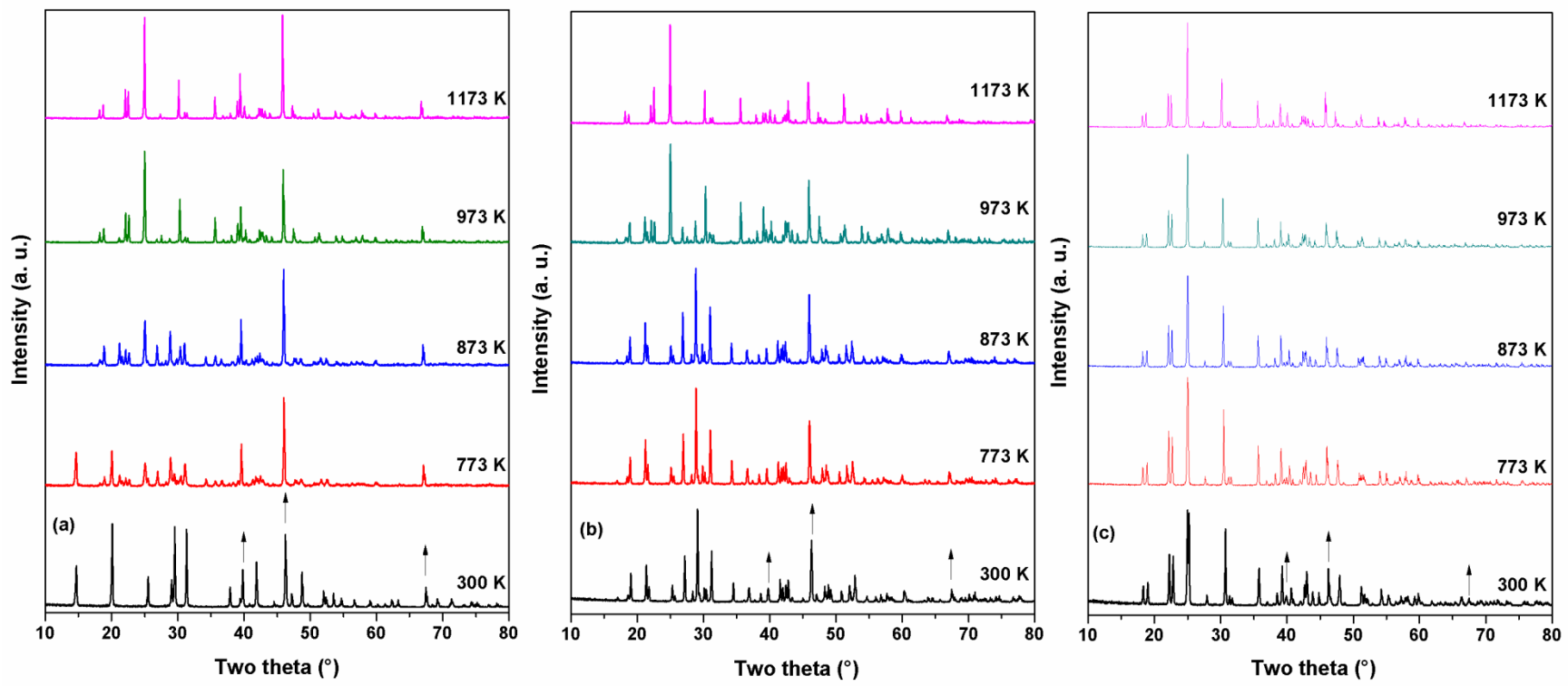

Fig. 5: Powder XRD patterns of $BiPO_4$ phases at representative temperatures. (a). Trigonal (I), (b). Monazite-type (II) and (c). $SbPO_4$-type (III) (↑ indicate platinum sample holder base peaks)

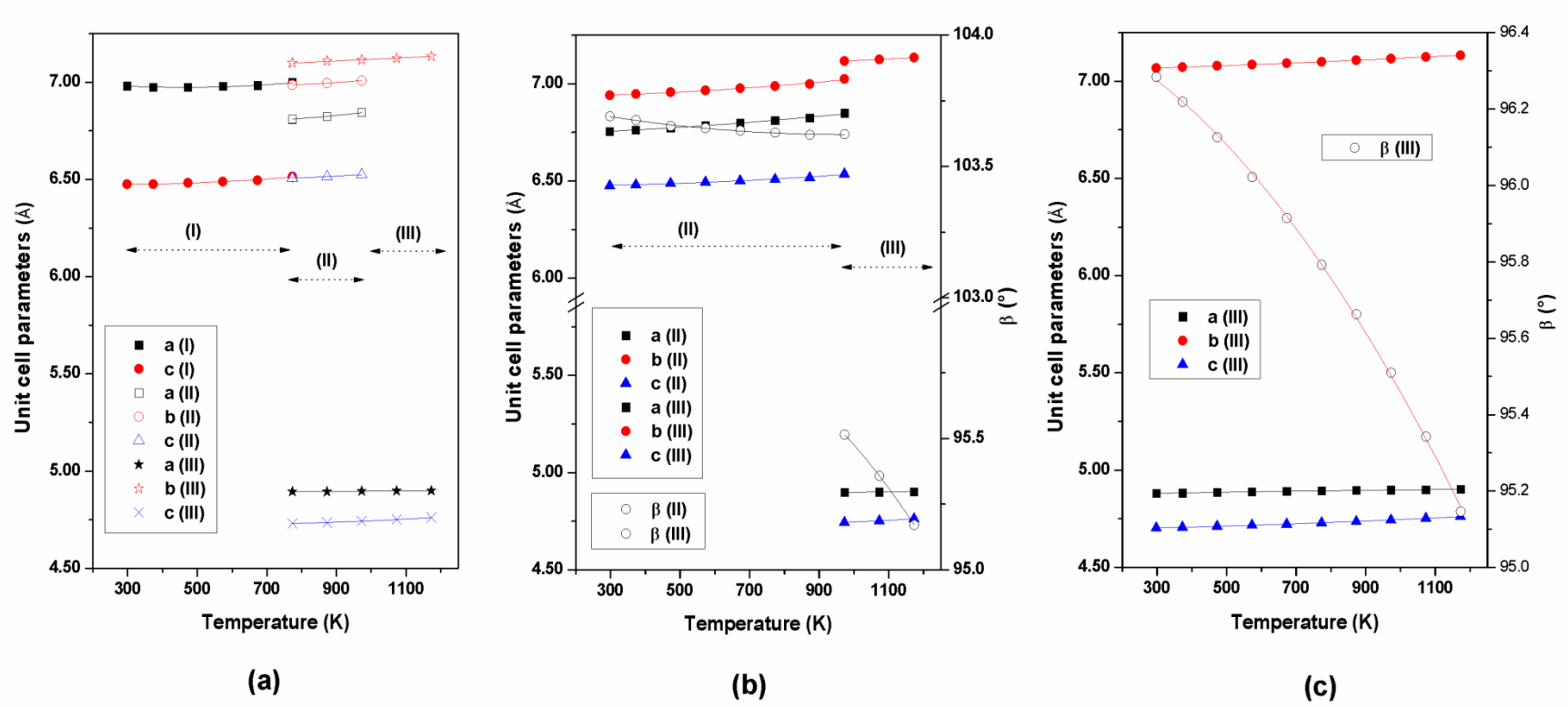

Fig. 6: Variation of unit cell parameters of $BiPO_4$ with temperature. (a). Trigonal (I), (b). Monazite-type (II) and (c). $SbPO_4$-type (III).

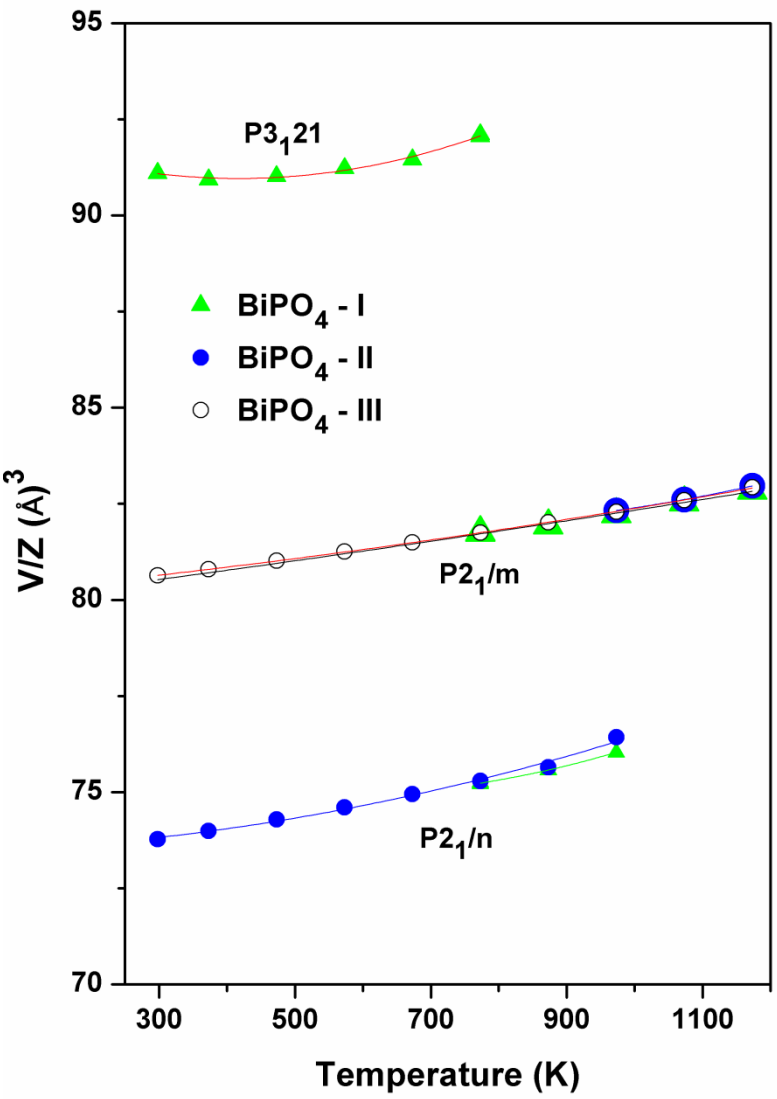

Fig. 7: Variation of molar volume of $BiPO_4$ phases with temperature.

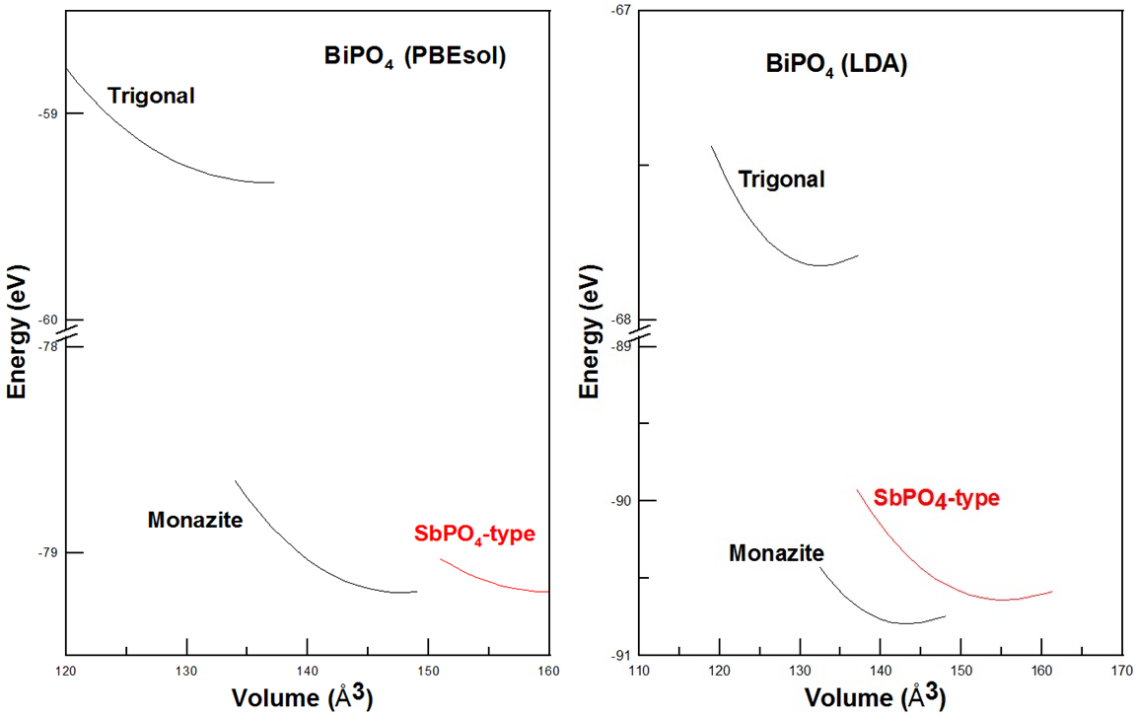

Fig. 8: Total energy as calculated by LDA and PBESol approach.

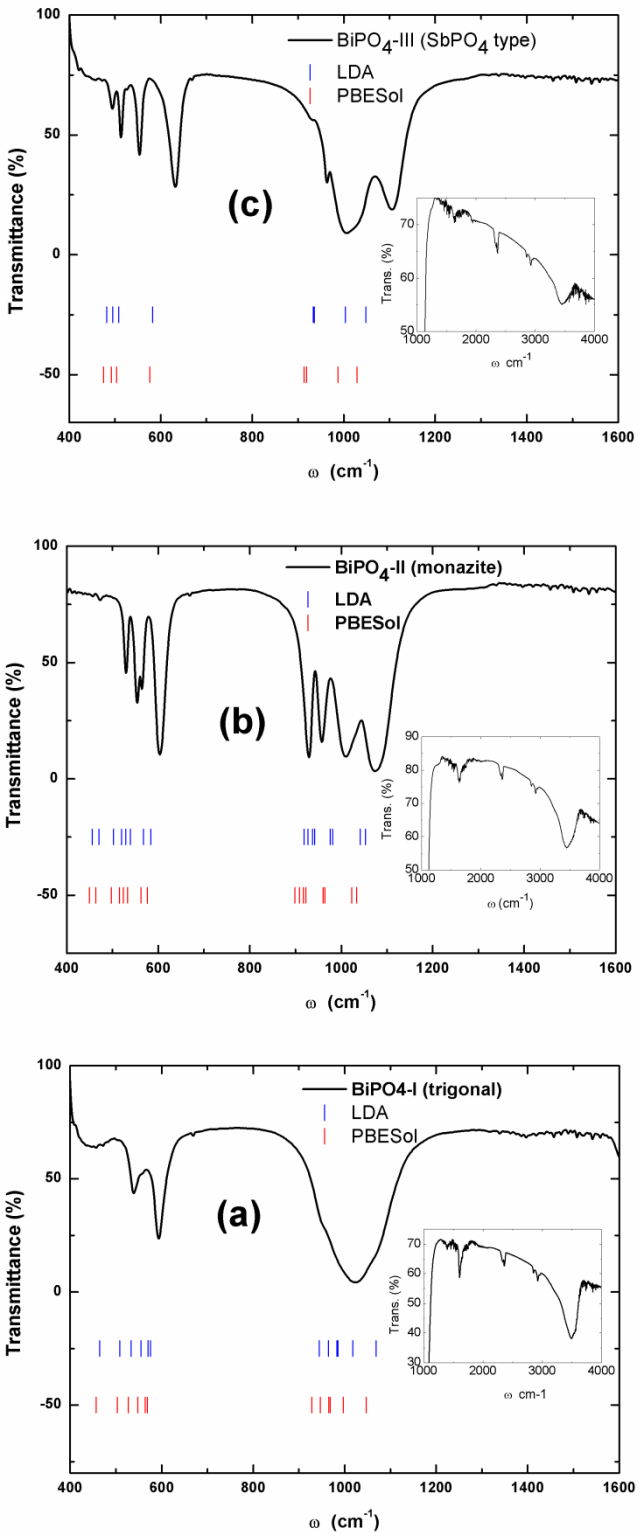

Fig. 9: Typical FTIR spectra of $BiPO_4$ phases. (a). Trigonal (I), (b). Monazite-type (II) and (c). $SbPO_4$-type (III). Vertical ticks indicate the calculated frequencies.

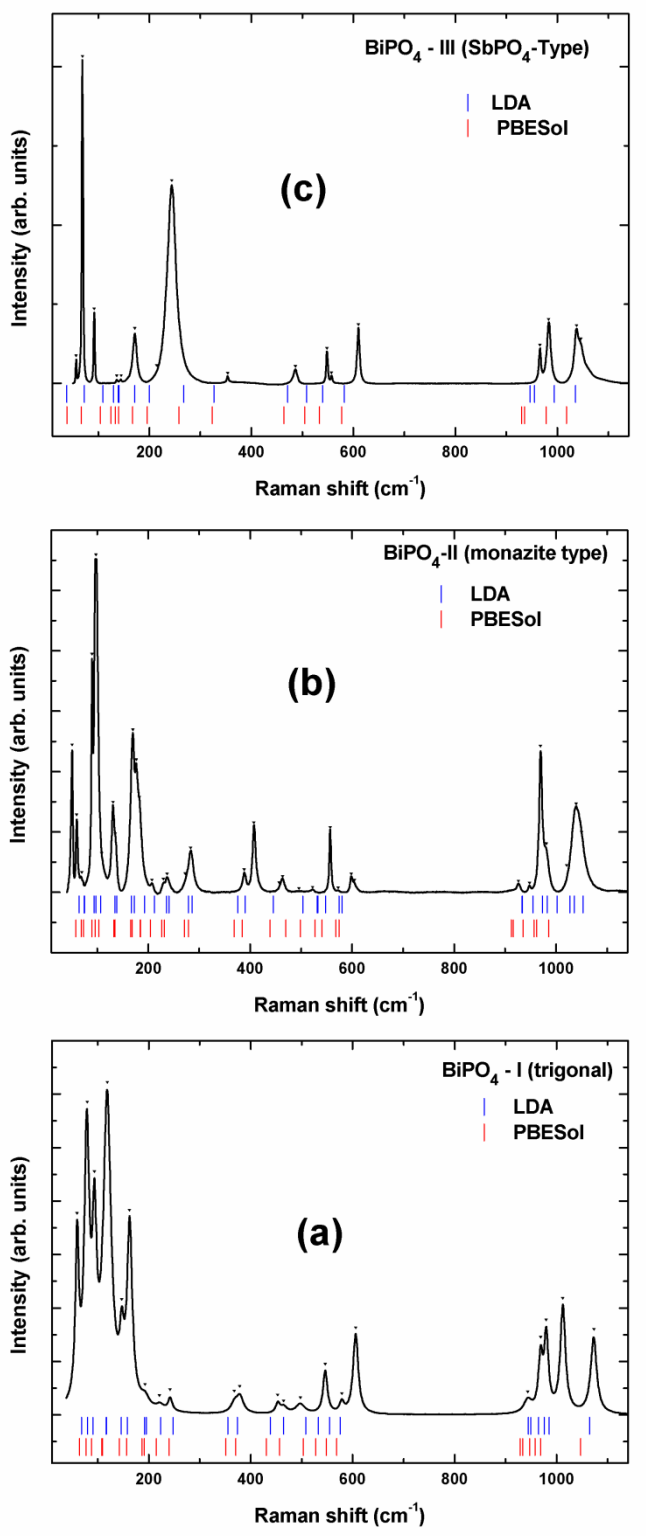

Fig. 10: Typical Raman spectra of $BiPO_4$ phases. (a). Trigonal (I), (b). Monazite-type (II) and (c). $SbPO_4$-type (III). Vertical ticks indicate the calculated frequencies.

(ν_4 bands) cm^{-1}. Additional new bands at 669, 632 cm^{-1} might be arising from the ν_3 and ν_1 modes of PO_4 units.

As regards Raman scattering measurements of $BiPO_4$ polymorphs presented in **Fig. 10**, it must be emphasized here that Raman data of $BiPO_4$ already reported in the literature are obscure in its interpretation, though they have been often used to characterize the $BiPO_4$ phases. [16-19, 32, 58, 59] In most cases, the high-frequency Raman modes of free PO_4 units were used to characterize the different phases, but a complete mode analysis has not been undertaken to our knowledge. Here we present a detailed symmetry analysis and computational study which has allowed us to identify almost all the Raman modes of the $BiPO_4$ phases (see **Table 5(a-c)**). In the present study, about 20 modes could be clearly identified in the Raman spectra of $BiPO_4$-I. As expected, internal vibrational modes of PO_4 units appear at high frequencies, while those due to the internal modes of the BiO_8 units are observed at low frequency. The intense A_1 (118.7 cm^{-1}, strong and sharp) and E (241.7 cm^{-1}, strong and broad) modes are due to the internal modes of BiO_8 polyhedra in $BiPO_4$-I. [60] The five modes observed at 944, 969, 980, 1012 and 1073 cm^{-1} are assigned to the symmetric and asymmetric stretching frequencies of P-O bonds of PO_4 units of the trigonal phase. Similar comparison with the earlier reported Raman modes of PO_4 groups, the bands observed at 498, 546, 579 and 606 cm^{-1} can be assigned to the bending (ν4) modes and bands at 379, 453, 465 cm^{-1} can be assigned to the (ν2) bending modes of PO_4 units. The stretching modes of bonds in PO_4 units in monazite (II) phase are also quite similar to those observed for trigonal (I) phase except that for some splitting. This can be attributed to highly dissimilar bond lengths in phases-I and II as described in the explanation of IR results. Similar split bands are also observed at lower frequencies due to the internal modes of the BiO_n units of phase II and III. In particular the phase II and III display an additional band around 400 cm^{-1} compared to the trigonal (I) phase. Earlier, such band was observed by Geng et al. [58] and Frost et al. [60] and had been assigned to the Bi-O stretching frequency of BiO_n polyhedra. This intensity and shift in the frequencies can be assigned to the average Bi-O bond length and compactness of the polyhedra as the structure changes from trigonal to monazite-type or $SbPO_4$-type structures.

5. Conclusions

In summary, the detailed analyses of the powder X-ray and neutron diffraction data as well as IR and Raman studies on three polymorphs of $BiPO_4$ revealed accurate structural parameters and local distortions parameters around $Bi^{3+}$and P^{5+}. Further the structural parameters and vibrational frequencies were supported by *ab initio* calculations based on DFT. The irreversible trigonal-monazite-$SbPO_4$-type structural transitions are explained from the molar volume and total energy of the three phases. Highly distorted structural arrangement around Bi^{3+} and P^{5+} has a very limited stability and is only stabilized by water molecules in the trigonal phase. It is revealed that structural transition from trigonal to monazite or $SbPO_4$ type structures is accompanied by a significant reduction in volume. DFT calculations revealed that the monazite and $SbPO_4$-type $BiPO_4$ have almost similar total energy and hence a competing stability. Further it is observed that monazite type phase shows larger lattice thermal expansion compared to the $SbPO_4$-type phase and thus it is truly a metastable phase.

Acknowledgements

This study was supported by the Spanish government MEC under Grants No: MAT2010-21270-C04-01/04, by MALTA Consolider Ingenio 2010 project (CSD2007-00045), and by the Vicerrectorado de Investigación y Desarrollo of the Universidad Politécnica de Valencia (UPV2011-0914 PAID-05-11 and UPV2011-0966 PAID-06-11). S.N.A. acknowledges the support provided by Universitat de Valencia during his visit to it. A.M. and P.R-H. acknowledge computing time provided by Red Española de Supercomputación (RES) and MALTA-Cluster.

†Electronic Supplementary Information (ESI) available: [(ESI-1). Further details of crystal structural data of the BiPO4-I, II and III can be obtained from the Fachinformationszentrum Karlsruhe, Abt. PROKA, 76344 Eggenstein-Leo-poldshafen, Germany (fax +49-7247-808-666; E-mail: crysdata@fiz-karlsruhe.de) on quoting the depository numbers CSD 426230 to 426255 (26 structures)]. See DOI: 10.1039/b000000x

References

1. L. A. Boatner and B. C. Sales, in “Radioactive Waste Forms for the Future” **1988,** p. 495. Eds. W. Lutze and R. C. Ewing, North-Holland, Amsterdam.
2. L. Bois, M. J. Guitter, F. Crrot, P. Trocellier, and M. Gautier-Soyer, *J. Nucl. Mater.* **2001**, *297*, 129.
3. N. Dacheux, A. C. Thomas, V. Brandel, and M. Genet, *J. Nucl. Mater.* **1998**, *257*, 108.
4. N. Clavier, N. Dacheux, and N. Podor, *Inorg. Chem.* **2006**, *45*, 220.
5. N. Clavier, N. Dacheux, C. Wallez, and M. Quarton, *J. Nucl. Mater.* **2006**, *352*, 209.
6. K. R. ELaud and F. A. Hummel, *J. Am. Ceram. Soc.* **1971**, *54*, 296.
7. O. Muller and R. Roy, *The Major Ternary Structural Families* (Springer, Berlin, **1974**).
8. M. J. Kohn, J. Rakovan, and J. M. Hughes, *Phosphates: Geochemical, Geobiological, and Materials Importance, vol. 48, p. 87–123. (Ed), Reviews in Mineralogy and Geochemistry, Mineralogical Society of America and the Geochemical Society, Chantilly, Virginia.*
9. D. Errandonea and F. J. Manjon, *Prog. Mater.* Sci. **2008**, *53*, 711.
10. O. Fukunaga and S. Yamaoka, *Phys. Chem. Miner* **1979**, *5*, 167.
11. E. H. Oelkers and J. –M. Montel, *Elements* **2008**, *4*, 113.
12. G. J. McCarthy, W. B. White, R. Roy, B. E. Scheetz, S. Komarneni, S. K. Smith, and D. M. Roy, *Nature* **1978**, *273*, 316.
13. G. J. McCarthy, W. B. White, and D. E. Pfoertsch, *Mater. Res. Bull.* **1978**, *13*, 1239.
14. I. -S. Cho, G. K. Choi, J. -S. An, J. -R. Kim, and K. S. Hong, *Mater. Res. Bull.* **2009**, *44*, 173.
15. N. Kitamura, K. Amezawa, Y. Tomii, and N. Yamamotoa, *Sol. State Ionics* **2003**, *161*,162.
16. C. Pan, D. Li, X. Ma, Y. Chen, and Y. Zhu, *Catal. Sci. Tech.* **2011**, *1*, 1399.
17. C. Pan, J. Xu, Y. Chen, and Y. Zhu, *Appl. Catal. B: Environmental* **2012**, *115*, 314.
18. M. Zhao, G. Li, J. Zheng, L. Li, H. Wang, and L. Yang, *Cryst. Engg* **2011**, *13*, 6251.
19. P. Arunkumar, C. Jayajothi, D. Jeyakumar, and N. Lakshminarasimhan, *RSC Adv* **2012**, *2*, 1477.
20. V. G. Alekseev, I. P. Gorelov, and M. V. Kornilov, *J. Anal. Chem.* **2000**5, *5*, 1055.

21. I. -S. Cho, J. R. Kim, D. W. Kim, and K. S. Hong, *J. Electroceram* **2006,** *16*, 379.
22. Z. Holgye and R. Poliak, *J. Radioanal. Nucl. Chem*. **1991**, *153*, 267.
23. Z. Holgye, *J. Radioanal. Nucl. Chem* **1998**, *12*, 227.
24. C. Pan and Y. Zhu, *Environ. Sci*. *Technol* **2010,** *44*, 5570.
25. C. Pan and Y. Zhu, Y. *J. Mater. Chem.* **2011**, *21*, 4235.
26. R. C. L. Mooney-Slater, *Z. Krist.* **1972**, *117*, 371.
27. G. Chiari and G. Ferraris, *Acta Cryst. B* **1982,** *38*, 2331.
28. M. Roming and C. Feldmann, *J. Mater. Sci* **2009**, *44*, 1412.
29. Y. -F. Lin, H. –W. Chang, S. –Y. Lu, and C. W. Liu, *J. Phys. Chem. C* **2007**, *111*, 18538.
30. I.-S. Cho, J.-R. Kim, D.-W. Kim, and K. S. Hong, *J. Electroceram* **2006,** *16*, 379.
31. R. Masse and A. C. Durif, *C. R. acad of Sci. Paris*, **1985**, *300*, 349.
32. B. Romero, S. Bruque, M. A. G. Aranda, and J. E. Iglesias, *Inorg. Chem.* **1994**, *33*, 1869.
33. B. S. Naidu, B. Vishwanadh, V. Sudarsan, and R. K. Vatsa, *Dalton Trans* **2012**, *41*, 3194.
34. M. Zhao, L. Li, J. Zheng, L. Yang, and G. Li, *Inorg. Chem*. **2013**, *52*, 807.
35. A. C. Larson and R. B. van Dreele, GSAS: General Structure Analysis System. Los Alamos National Laboratory, Report LA-UR 86-748, **2000**.
36. J. Rodriguez-Carvajal, Fullprof 2000: A Program for Rietveld, Profile Matching and Integrated Intensity Refinements for X-ray and Neutron Data. Version 1.6, Laboratoire Leon Brillouin, Gif sur Yvette, France, **2000**.
37. G. Kresse and J. Furthmuller, *Phys. Rev. B* **1996**, *54*, 11169.
38. G. Kresse and D. Joubert, *Phys. Rev. B* **1999,** *59*, 1758.
39. P. E. Blochl, *Phys.Rev. B* **1994,** *50*, 17953.
40. J. P. Perdew and A. Zunger, *Phys. Rev. B*, **1981**, *23*, 5048.
41. J. P. Perdew, K. Burke, and M. Ernzerhof, *Phys. Rev. Lett.* **1996**, *77*, 3865.
42. A. Mujica, A. Rubio, A. Muñoz, and R. J. Needs, *Rev. Mod. Phys.* **2003**, *75*, 863.
43. K. Parlinski, computer code PHONON [http://wolf.ifj.edu.pl/phonon/].
44. F. Xue, H. Li, Y. Zhu, S. Xiong, X. Zhang, T. Wang, X. Liang, and Y. Qian, *J. Solid State Chem.* **2009**, *182*, 1396.
45. S. J. Patwe, S. N. Achary, and A. K. Tyagi, *J. Mater. Res.*, **2009**, *24*, 3551.
46. S. N. Achary, S. J. Patwe, M. D. Mathews, and A. K Tyagi, *J. Phys. Chem. Solids*, **2006**, *67*, 774.

47. S. J. Patwe, S. N. Achary, and A. K. Tyagi, *Am. Mineralogist*, 2009, 94, 98.
48. R. Lacomba-Perales, D. Errandonea, Y. Meng, and M. Bettinelli, *Phys. Rev. B* **2010**, *81*, 064113.
49. V. Panchal, S. López-Moreno, D. Santamaŕıa-Pérez, D. Errandonea, D. J. Manóon, P. Rodŕguez-Hernandez, A. Mũnoz, S. N. Achary, and A. K. Tyagi, *Phys. Rev. B* **2011**, 84, 024111.
50. D. Errandonea, R. S. Kumar, S. N. Achary, and A. K. Tyagi, *Phys. Rev. B* **2011**, *84*, 224121.
51. L. Gracia, A. Beltran, D. Errandonea, and J. Andres, *Inorg. Chem.* **2012**, *51*, 1751.
52. T. B. Zunic and L. Vickovic, *J. Appl. Cryst.* **1996**, *29*, 305.
53. E. Makovicky and T. B. Zunic, *Acta Cryst. B* **1998**, *54*, 766.
54. M. E. Poloznikova and V. V. Fomichev, *Usp. Khim.*, **1994**, *63*, 419.
55. L. Baia, R. Stefan, W. Kiefer, J. Popp, and S. Simon, *J. Non-Cryst. Solids*, **2002**, *303*, 379.
56. S. D. Ross, *Inorganic Infrared and Raman Spectra* (McGraw-Hill, London, **1972**).
57. K. Nakamoto, Infrared and Raman spectra of Inorganic and Coordination Compounds (Wiley, New York, **1986**).
58. J. Geng, W. H. Hou, Y. N. Lv, J. J. Zhu, and H. Y. Chen, *Inorg. Chem.* **2005**, *44*, 8503.
59. G. M. Begun, G. W. Beall, L. A. Boatner, and W. J. Gregor, *J. Raman Spect.* **1981**, *11*, 273.
60. R. L. Frost, M. L. Weier, K. L. Erickson, O. Carmody, and S. J. Mills, *J. Raman Spect.* **2004**, *35*, 1047.

Figure Captions

Fig. 1: Powder XRD patters of different phases of $BiPO_4$ at ambient temperature ($\lambda = 1.5417$Å).

Fig. 2: Rietveld refinement plots of powder neutron diffraction data of $BiPO_4$ phases, (a). Trigonal (I), (b). Monazite-type (II) and (c). $SbPO_4$-type (III). ($\lambda = 1.249$ Å).

Fig. 3: Crystal structure of $BiPO_4$ phases, (a). Trigonal (I), (b). Monazite-type (II) and (c). $SbPO_4$-type (III). (BiO_8 (in a and c), BiO_9 (in b) and PO_4 units are shown). (isolated spheres are O3(of water molecules in $BiPO_4$-I).

Fig. 4: Typical coordination around Bi^{3+} in $BiPO_4$ phases, (a). Trigonal (I), (b). Monazite type (II) and (c). $SbPO_4$ type (III)

Fig. 5: Powder XRD patterns of $BiPO_4$ phases at representative temperatures. (a). Trigonal (I), (b). Monazite-type (II) and (c). $SbPO_4$-type (III) (↑ indicate platinum sample holder base peaks)

Fig. 6: Variation of unit cell parameters of $BiPO_4$ with temperature. (a). Trigonal (I), (b). Monazite-type (II) and (c). $SbPO_4$-type (III).

Fig. 7: Variation of molar volume of $BiPO_4$ phases with temperature.

Fig. 8: Total energy as calculated by LDA and PBESol approach.

Fig. 9: Typical FTIR spectra of $BiPO_4$ phases. (a). Trigonal (I), (b). Monazite-type (II) and (c). $SbPO_4$-type (III). Vertical ticks indicate the calculated frequencies.

Fig. 10: Typical Raman spectra of $BiPO_4$ phases. (a). Trigonal (I), (b). Monazite-type (II) and (c). $SbPO_4$-type (III). Vertical ticks indicate the calculated frequencies.

Tables

Table 1: Refined unit cell parameters for different polymorphs of $BiPO_4$ at ambient temperature (300K). (Calculated unit cell parameters are also included for comparison)

Table-2: Refined and calculated structural parameters of $BiPO_4$ at 300K ((a). Trigonal (I), (b). Monazite-type (II) and (c). $SbPO_4$-type (III)).

Table 3: The typical bond lengths and polyhedral parameters in different phases of $BiPO_4$.

Table 4: Calculated and observed Infrared modes of different $BiPO_4$ phases. ((a). Trigonal (I), (b). Monazite-type (II) and (c). $SbPO_4$-type (III).)

Table 5: Calculated and observed Raman modes of $BiPO_4$ phases. ((a). Trigonal (I), (b). Monazite-type (II) and (c). $SbPO_4$-type (III)).

Table 1: Refined unit cell parameters for different polymorphs of $BiPO_4$ at ambient temperature (300K). (Calculated unit cell parameters are also included for comparison)

	$BIPO_4$-I $BiPO_4$ 0.67 H_2O (trigonal)				$BIPO_4$-II $BiPO_4$ (Monazite-type)				$BIPO_4$-III $BiPO_4$ ($SbPO_4$-type)			
	Space group: $P3_121$ (No. 152)				*Space group:*$P2_1/n$ (No. 14)				*Space group:*$P2_1/m$ (No. 11)			
	ND	XRD	LDA	PBESol	ND	XRD	LDA	PBESol	ND	XRD	LDA	PBESol
a (Å)	6.9793(5)	6.9813(2)	6.9151	6.9882	6.7561(4)	6.7552(1)	6.6658	6.7549	4.8807(2)	4.8804(1)	4.7375	4.7809
b (Å)					6.9408(4),	6.9417(2)	6.8869	6.9551	7.0674(3)	7.0684(2)	7.0726	7.1590
c (Å)	6.4743(7)	6.4751(2)	6.3798	6.4314	6.4764(3)	6.4772(2)	6.4148	6.4700	4.7023(2)	4.7033(1)	4.6387	4.7011
β (°)					103.695(5)	103.691(2)	103.79	103.95	96.303(4)	96.285(3)	95.91	96.07
V ($Å^3$)	273.11(3)	273.31(1)	264.20	272.00	295.06(2	295.10(1)	286.00	295.00	161.22(1)	161.27(1)	154.6	160.00
Z	3				4				4			
V/Z ($Å^3$)	91.04				73.77				80.61			
R_p, R_{wp}	0.0164, 0.0216				0.0276, 0.0351				0.0385; 0.0517			
χ^2	0.096				1.073				2.027			
R_F^2	0.0813				0.0578				0.0428			

.

Table-2: Refined and calculated structural parameters of $BiPO_4$ at 300K ((a). Trigonal (I), (b). Monazite-type (II) and (c). $SbPO_4$-type (III)).

(a). $BiPO_4$-I. (Trigonal)

	wyc	***x***	***y***	***z***	***occ***	***Uiso Å²***
Bi	*3b*	**0.4703(9)**	**0**	**5/8**	**1**	**0.0077(13)**
		0.47727	*0.00000*	*0.83333*		
		0.48136	0.00000	0.83333		
P	*3a*	**0.4401(15)**	**0**	**1/3**	**1**	**0.0093(17)**
		0.44011	*0.00000*	*0.33333*		
		0.44194	0.00000	0.33333		
O1	*6c*	**0.3939(12)**	**0.1569(15)**	**0.4592(10)**	**1**	**0.0231(18)**
		0.60625	*0.15651*	*0.19788*		
		0.60569	0.15485	0.19843		
O2	*6c*	**0.6270(12)**	**0.1324(12)**	**0.1652(11)**	**1**	**0.0152(17)**
		0.49845	*0.12767*	*0.49385*		
		0.49651	0.12678	0.49308		
O3(w)	*6c*	**0.064(9)** *	**0.090(10)**	**0.392(8)**	**0.335**	**0.011(5)**

1st row : Refined parameters from powder neuron diffraction data
2nd row : LDA (a = b = 6.91509 Å, c = 6.37979 Å, γ = 120º)
3rd row : PBESol. (a = b = 6.98821 Å, c = 6.43141 Å, γ = 120º)
(Calculated Structures at 0 pressure and 0 K)
* Note that in the trigonal structure we neglected the presence of the H_2O molecule in calculations.

(b). $BiPO_4$-II (Monazite-type)

	wyc	*x*	*y*	*z*	*occ*	*Uiso (Å^2)*
Bi	*4e*	**0.2871(5)**	**0.1447(5)**	**0.0859(5)**	**1**	**0.0092(6)**
		0.2824	*0.1462*	*0.0906*		
		0.28394	0.14513	0.08817		
P	*4e*	**0.2966(8)**	**0.1615(5)**	**0.6163(7)**	**1**	**0.0073(9)**
		0.2995	*0.1622*	*0.6141*		
		0.29933	0.16215	0.61291		
O1	*4e*	**0.2617(6)**	**0.0003(6)**	**0.4459(8)**	**1**	**0.0110(9)**
		0.2594	*0.0041*	*0.4411*		
		0.25990	0.00537	0.44010		
O2	*4e*	**0.3771(6)**	**0.3410(7)**	**0.5143(6)**	**1**	**0.0067(7)**
		0.3799	*0.3422*	*0.5148*		
		0.37939	0.34210	0.51574		
O3	*4e*	**0.4618(6)**	**0.1029(7)**	**0.8136(7)**	**1**	**0.0025(8)**
		0.4664	*0.1027*	*0.8189*		
		0.46480	0.10182	0.81782		
O4	*4e*	**0.1161(7)**	**0.2011(7)**	**0.7097(7)**	**1**	**0.0067(9)**
		0.1144	*0.2059*	*0.7113*		
		0.11546	0.20505	0.70932		

1st row : Refined parameters from powder neuron diffraction data
2nd row : LDA ($P2_1/n$, setting 7) a = 6.6658 Å, b = 6.8869 Å, c = 6.4148 Å, β = 103.79º)
3rd row : PBESol. ($P2_1/n$, setting 7) a = 6.7549 Å, b = 6.9551 Å, c = 6.4700 Å, β = 103.95º)
(Calculated structures at 0 pressure and 0 K)

(c). $BiPO_4$-III ($SbPO_4$-type)

	wyc	*x*	*y*	*z*	*occ*	*Uiso* ($Å^{2)\#}$
Bi	2e	**0.1424(4)**	**0.2500**	**0.1671(5)**	**1**	**0.00875**
		0.12747	*0.25000*	*0.15446*		
		0.13160	0.25000	0.14926		
P	2e	**0.3733(7)**	**0.7500**	**0.3027(7)**	**1**	**0.00403**
		0.63319	*0.25000*	*0.67447*		
		0.63746	0.25000	0.67464		
O1	2e	**0.6761(5)**	**0.7500**	**0.2291(7)**	**1**	**0.01239**
		0.31724	*0.25000*	*0.72805*		
		0.32318	0.25000	0.72855		
O2	2e	**0.6013(6)**	**0.2500**	**0.3655(6)**	**1**	**0.01373**
		0.63648	*0.25000*	*0.34423*		
		0.64067	0.25000	0.34750		
O3	4f	**0.2102(4)**	**0.5802(4)**	**0.1750(5)**	**1**	**0.01231**
		0.20392	*0.57963*	*0.18037*		
		0.20006	0.58078	0.18053		

1st row : Refined parameters from powder neuron diffraction data
2nd row : LDA ($P2_1/m$, a = 4.73755 Å, b = 7.07260 Å, c = 4.63868 Å, β = 95.91397º)
3rd row : PBASol. ($P2_1/m$, a = 4.78092 Å, b = 7.15898 Å, c = 4.70108 Å, β = 96.06833º)
(Calculated Structures at 0 pressure and 0 K)

Anisotropic thermal parameters for $BiPO_4$ ($SbPO_4$-type)

	U_{11} ($Å^2$)	U_{12} ($Å^2$)	U_{13} ($Å^2$)	U_{22} ($Å^2$)	U_{23} ($Å^2$)	U_{33} ($Å^2$)
Bi	0.0129(13)	0.0	0.0003(9)	0.0022(13)	0.0	0.0110(11)
P	0.0051(16)	0.0	-0.0018(13)	0.0064(15)	0.0	0.0001(17)
O1	0.0014(14)	0.0	-0.0011(13)	0.0262(17)	0.0	0.0092(19)
O2	0.0059(16)	0.0	0.0042(15)	0.0228(19)	0.0	0.0132(19)
O3	0.0134(12)	0.0012(9)	-0.0037(9)	0.0101(12)	-0.0050(10)	0.0124(11)

Table 3: The typical bond lengths and polyhedral parameters in different phases of $BiPO_4$.

$BIPO_4$-I (Trigonal)		$BIPO_4$-II (Monazite-type)		$BIPO_4$-III ($SbPO_4$-type)	
Bi - O1	2.817(8) (Å)	Bi - O1	2.580(6) (Å)	Bi - O1	2.149(4) (Å)
Bi - O1	2.296(8)	Bi - O1	2.492(5)	Bi - O1	2.880(4)
Bi - O1	2.817(7)	Bi - O2	3.020(5)	Bi - O2	2.896(4)
Bi - O1	2.296(12)	Bi - O2	2.399(6)	Bi - O2	2.330(3)
Bi - O2	2.378(7)	Bi - O2	2.700(5)	Bi - O3	2.357(3)
Bi1 -O2	2.490(9)	Bi - O3	2.361(6)	Bi - O3	2.526(3)
Bi - O2	2.490(7)	Bi - O3	2.394(6)	Bi - O3	2.526(3)
Bi - O2	2.378(8)	Bi - O4	2.469(5))	Bi - O3	2.357(3)
		Bi - O4	2.426(6)		
CN:	6+2	CN	8+1	CN	8
<Bi-O>	2.495(3) (Å)	$<Bi-O>_9$	2.538(2) (Å)	<Bi-O>	2.503(1) (Å)
Distt.	62.976 $x10^{-4}$	Distt.	60.598 $x10^{-4}$	Distt.	98.915 $x10^{-4}$
		$<Bi-O>_8$	2.478(2) (Å)		
		Distt.	18.238 $x10^{-4}$		
V_{BiO8} ($Å^3$)	29.06	V_{BiO8} ($Å^3$)	26.26	V_{BiO8} ($Å^3$)	27.28
Distt.	0.1491	Distt.	0.0684	Distt.	0.0819
Sphericity	0.844	Sphericity	0.941	Sphericity	0.910
Eccentricity	0.346	Eccentricity	0.196	Eccentricity	0.449
		V_{BiO9} ($Å^3$)	31.95		
		Distt.	0.0557		
		Sphericity	0.853		
		Eccentricity	0.308		
P – O1	1.523(12) (Å)	P - O1	1.550(7) (Å)	P - O1	1.554(4) (Å)
P - O1	1.523(9)	P - O2	1.567(7)	P - O2	1.552(4)
P - O2	1.592(9)	P - O3	1.539(6)	P - O3	1.526(3)
P - O2	1.592(10)	P -O4	1.509(8)	P - O3	1.526(3)
$<P-O>_4$	1.558(5) (Å)	$<P-O>_4$	1.541(4) (Å)	<P-O>	1.540(2) (Å)
Distt.	4.895 $x10^{-4}$	Distt.	1.839 $x10^{-4}$	Distt.	0.757 $x10^{-4}$
V_{PO4} ($Å^3$)	1.923	V_{PO4} ($Å^3$)	1.862	V_{PO4} ($Å^3$)	1.861
Distt.	0.0128	Distt.	0.0094	Distt.	0.0070
Sphericity	1	Sphericity	1	Sphericity	1
Eccentricity	0.042	Eccentricity	0.066	Eccentricity	0.116

Table 4: Calculated and observed Infrared modes of different $BiPO_4$ phases. ((a). Trigonal (I), (b). Monazite-type (II) and (c). $SbPO_4$-type (III).)

(a). Trigonal ($BiPO_4$-I)

Mode	LDA ω (cm^{-1})	Mode	PBESol ω (cm^{-1})	Mode	Exp. ω (cm^{-1})
E(RI)	68.414	E(RI)	64.4806		
A2(I)	81.590	A2(I)	78.057		
E(RI)	90.897	E(RI)	87.931		
A2(I)	104.940	A2(I)	106.544		
E(RI)	116.314	E(RI)	107.578		
E(RI)	146.135	A2(I)	139.669		
A2(I)	147.536	E(RI)	142.2376		
E(RI)	157.944	E(RI)	156.448		
E(RI)	191.967	E(RI)	187.203		
A2(I)	205.210	A2(I)	195.776		
E(RI)	223.289	E(RI)	214.890		
E(RI)	247.906	E(RI)	240.042		
A2(I)	251.242	A2(I)	241.844		
E(RI)	355.281	E(RI)	351.190		
E(RI)	464.691	E(RI)	456.668	E(RI)	443b
E(RI)	508.088	E(RI)	503.035		
A2(I)	533.472	A2(I)	526.886	A2(I)	539s
E(RI)	554.754	E(RI)	548.035	E(RI)	553w
A2(I)	570.131	A2(I)	563.846	A2(I)	560w
E(RI)	575.401	E(RI)	568.750	E(RI)	594s
E(RI)	944.692	E(RI)	928.447		
E(RI)	964.640	E(RI)	946.861	E(RI)	949s
A2(I)	982.452	A2(I)	964.907		
E(RI)	985.354	E(RI)	968.176	E(RI)	957s
A2(I)	1017.977	A2(I)	996.597		
E(RI)	1068.679	E(RI)	1047.101	E(RI)	1023s
					1065s

(b). Monazite-type ($BiPO_4$-II)

Mode	LDA ω (cm^{-1})	Mode	PBESol ω (cm^{-1})	Mode	Exp. ω (cm^{-1})
Au(I)	71.850	Au(I)	65.915		
Bu(I)	83.258	Bu(I)	75.555		
Au(I)	86.527	Au(I)	83.395		
Bu(I)	112.812	Bu(I)	102.976		
Au(I)	124.053	Au(I)	112.116		
Bu(I)	154.208	Bu(I)	147.041		
Au(I)	157.143	Au(I)	154.447		
		Bu(I)	172.493		
Au(I)	179.859	Au(I)	174.495		
Bu(I)	180.059				
Bu(I)	194.436	Bu(I)	188.305		
Au(I)	208.746	Au(I)	203.716		
Bu(I)	217.652	Bu(I)	213.757		
Au(I)	236.999	Au(I)	227.967		
		Au(I)	254.186		
Bu(I)	260.915	Bu(I)	256.421		
Au(I)	262.483				
Bu(I)	366.722	Bu(I)	359.430		
Au(I)	368.957	Au(I)	363.934		
Au(I)	455.618	Au(I)	449.496		
Bu(I)	470.295	Bu(I)	463.373	Bu(I) + Bu(I)	473w
Au(I)	502.284	Au(I)	497.932		
Bu(I)	519.996	Bu(I)	514.844		
Au(I)	528.802	Au(I)	523.784	Au(I)	529s
Bu(I)	539.276	Bu(I)	533.091	Bu(I)	554s
Bu(I)	567.996	Bu(I)	562.579	Bu(I)	564s
Au(I)	583.440	Au(I)	576.756	Au(I)	604s
Bu(I)	919.141	Bu(I)	898.993	Bu(I)	876w
Au(I)	927.614	Au(I)	908.867		
Au(I)	937.154	Au(I)	917.306		
Bu(I)	941.690	Bu(I)	922.276	Bu(I)	930s
Bu(I)	975.847	Bu(I)	960.671	Bu(I)	958s
Au(I)	981.151	Au(I)	963.974		
Bu(I)	1041.426	Bu(I)	1023.317	Bu(I)	1011s
Au(I)	1052.968	Au(I)	1033.925	Au(I)	1031s
					1076s

(c). $SbPO_4$-type ($BiPO_4$-III).)

Mode	LDA ω (cm^{-1})	Mode	PBESol ω (cm^{-1})	Mode	Exp.ω (cm^{-1})
Bu(I)	120.184	Bu(I)	109.080		
Au(I)	126.955	Au(I)	113.516		
Bu(I)	153.507	Bu(I)	149.909		
Au(I)	185.196	Au(I)	182.7673		
Bu(I)	201.340	Bu(I)	196.410		
Au(I)	209.880	Au(I)	203.616		
Au(I)	322.725	Au(I)	320.468		
					421w
					434w
					451w
					457w
Bu(I)	481.869	Bu(I)	474.848	Bu(I)	472w
Au(I)	494.545	Au(I)	491.860	Au(I)	494s
Bu(I)	508.088	Bu(I)	503.702	Bu(I)	513s
					527w
Bu(I)	582.373	Bu(I)	576.222	Bu(I)	554s
					630s
Au(I)	933.651	Au(I)	913.670		
Bu(I)	936.120	Bu(I)	918.707	Bu(I)	928w
				Bu(I)	963s
Bu(I)	1003.333	Bu(I)	987.624	Bu(I)	1005s
Bu(I)	1048.631	Bu(I)	1029.521	Bu(I)	1029s
					1105s

Table 5: Calculated and observed Raman modes of $BiPO_4$ phases. ((a). Trigonal (I), (b). Monazite-type (II) and (c). $SbPO_4$-type (III)).

(a). Trigonal ($BiPO_4$-I),

Mode	LDA - ω (cm^{-1})	Mode	PBESol ω (cm^{-1})	Modes	Exper. - ω (cm^{-1})
E(RI)	68.414	E(RI)	64.480		
A1(R)	79.922	A1(R)	77.223		
E(RI)	90.897	E(RI)	87.931	E(RI)	93.6
E(RI)	116.314	E(RI)	107.578		
A1(R)	117.148	A1(R)	109.780	A1(R)	118.7
E(RI)	146.135	E(RI)	142.237	E(RI)	146.9
E(RI)	157.944	E(RI)	156.448	E(RI)	162.2
E(RI)	191.967	E(RI)	187.203	E(RI)	192.6
A1(R)	195.303	A1(R)	191.273		
E(RI)	223.289	E(RI)	214.890	E(RI)	220.8
E(RI)	247.906	E(RI)	240.042	E(RI)	241.7
E(RI)	355.281	E(RI)	351.190	E(RI)	367.9
A1(R)	373.494	A1(R)	370.705	A1(R)	378.8
A1(R)	438.506	A1(R)	430.515	A1(R)	452.8
E(RI)	464.691	E(RI)	456.668	E(RI)	464.7
E(RI)	508.088	E(RI)	503.035	E(RI)	497.5
A1(R)	532.938	A1(R)	527.186	A1(R)	546.4
E(RI)	554.754	E(RI)	548.035	E(RI)	579
E(RI)	575.401	E(RI)	568.750	E(RI)	606.2
E(RI)	944.692	E(RI)	928.447	E(RI)	943.7
A1(R)	949.162	A1(R)	933.217		
E(RI)	964.640	E(RI)	946.861	E(RI)	968.8
A1(R)	975.881	A1(R)	957.735	A1(R)	979.7
E(RI)	985.354	E(RI)	968.176	E(RI)	1012
E(RI)	1068.679	E(RI)	1047.101	E(RI)	1073.4

(b). Monazite-type ($BiPO_4$-II)

Mode	LDA ω (cm^{-1})	Mode	PBESol ω (cm^{-1})	Mode	Exper ω (cm^{-1})
Ag(R)	64.378	Ag(R)	58.209	Ag	50,9
Ag(R)	74.285	Ag(R)	68.383	Ag	59,8
Bg(R)	75.286	Bg(R)	73.287	Bg	69,9
Bg(R)	93.699	Bg(R)	89.332	Bg	89,6
Ag(R)	97.335	Ag(R)	95.337	Ag	97,3
Bg(R)	106.908	Bg(R)	102.642	Bg	108,6
		Ag(R)	132.697	Bg	131,1
Bg(R)	134.561	Bg(R)	134.732	Bg	135,5
Ag(R)	138.597				
Ag(R)	166.950	Ag(R)	165.688	Ag	169,9
Bg(R)	172.921	Bg(R)	167.790	Bg + Ag	176,7
Ag(R)	172.787	Ag(R)	168.424		
Ag(R) + Bg(R)	192.601	Ag(R)	184.002	Ag + Bg	182,7
		Bg(R)	185.236		
Bg(R)	212.115	Bg(R)	203.883	Bg	207,4
Bg(R)	235.931	Bg(R)	226.199	Bg	229,8
Ag(R)	240.434	Ag(R)	231.903	Ag	237,1
Bg(R)	279.095	Bg(R)	271.332	Bg	272,5
Ag(R)	286.133	Ag(R)	278.671	Ag	283,5
Bg(R)	375.729	Bg(R)	368.303	Bg	388,4
Ag(R)	390.439	Ag(R)	384.549	Ag	407,4
Ag(R)	445.077	Ag(R)	438.688	Ag	457,0
Bg(R)	477.833	Bg(R)	469.945	Bg	463,5
Ag(R)	503.051	Ag(R)	497.999	Ag	495,9
Ag(R)	531.404	Ag(R)	527.220	Ag	522,7
Bg(R)	532.638	Bg(R)	527.287	Bg	557,1
Bg(R)	547.749	Bg(R)	540.930	Bg	572,6
Ag(R)	573.867	Ag(R)	568.083	Ag	598,3
Bg(R)	580.405	Bg(R)	573.921	Bg	604,5
Ag(R)	933.184	Ag(R)	911.936	Ag + Bg	926,3
Bg(R)	933.685	Bg(R)	915.772		
Ag(R)	954.933	Ag(R)	935.286	Ag	947,8
Ag(R)	973.412	Ag(R)	956.502	Ag	969,5
Bg(R)	982,552	Bg(R)	962.272	Bg	981,0
Bg(R)	1001.799	Bg(R)	985.256	Bg	1021,0
Ag(R)	1027.383	Ag(R)	1010.141	Ag	1039,4
Bg(R)	1035.389	Bg(R)	1016.612	Bg	1050,2

(c). $SbPO_4$-type ($BiPO_4$-III).)

Mode	LDA ω (cm^{-1})	Mode	PBESol ω (cm^{-1})	Modes	Exper. ω (cm^{-1})
Ag(R)	37.793	Ag(R)	38.294	Ag(R)	56.2
Ag(R)	72.050	Ag(R)	66.315	Ag(R)	68.8
Bg(R)	108.843	Bg(R)	103.842	Bg(R)	91.7
Ag(R)	129.424	Ag(R)	124.624		
Bg(R)	138.763	Ag(R)	132.830	Ag(R)	135.7
Ag(R)	140.465	Bg(R)	139.835	Bg(R)	144.5
Bg(R)	171.553	Bg(R)	166.922	Bg(R)	171.2
Ag(R)	200.240	Ag(R)	195.710	Ag(R)	214.2
Bg(R)	267.420	Bg(R)	258.022	Bg(R)	244
Bg(R)	326.328	Bg(R)	322.936	Bg(R)	353.6
Ag(R)	470.762	Ag(R)	463.573	Ag(R)	486.4
Ag(R)	508.221	Ag(R)	504.403	Ag(R)	548.3
Bg(R)	539.310	Bg(R)	533.724	Bg(R)	557.1
Ag(R)	582.139	Ag(R)	576.856	Ag(R)	609.9
Ag(R)	946.694	Ag(R)	929.982	Ag(R)	966.1
Bg(R)	955.200	Bg(R)	936.019	Bg(R)	982.9
Ag(R)	994.327	Ag(R)	978.050	Ag(R)	1037.8
Ag(R)	1035.589	Ag(R)	1017.946	Ag(R)	1046

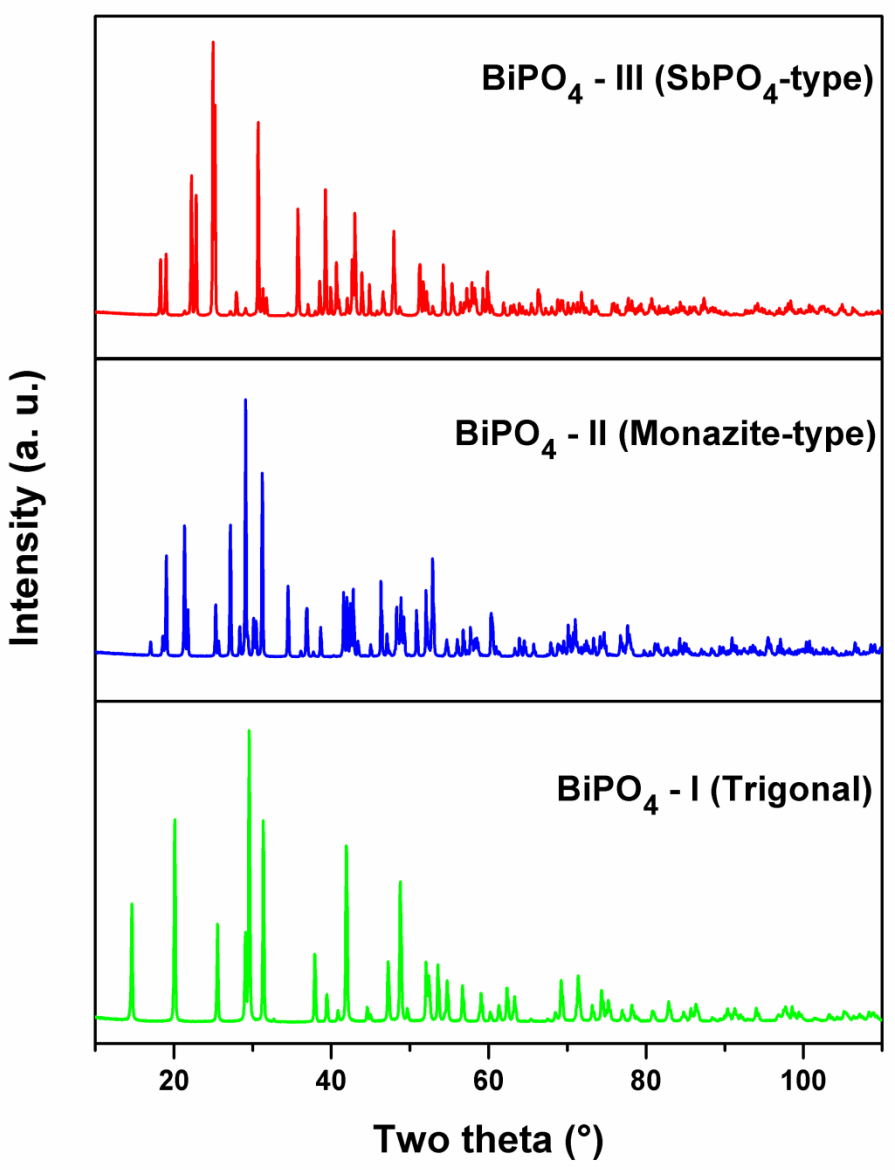

Fig. 1: Powder XRD patters of different phases of $BiPO_4$ at ambient temperature ($\lambda = 1.5417$Å).

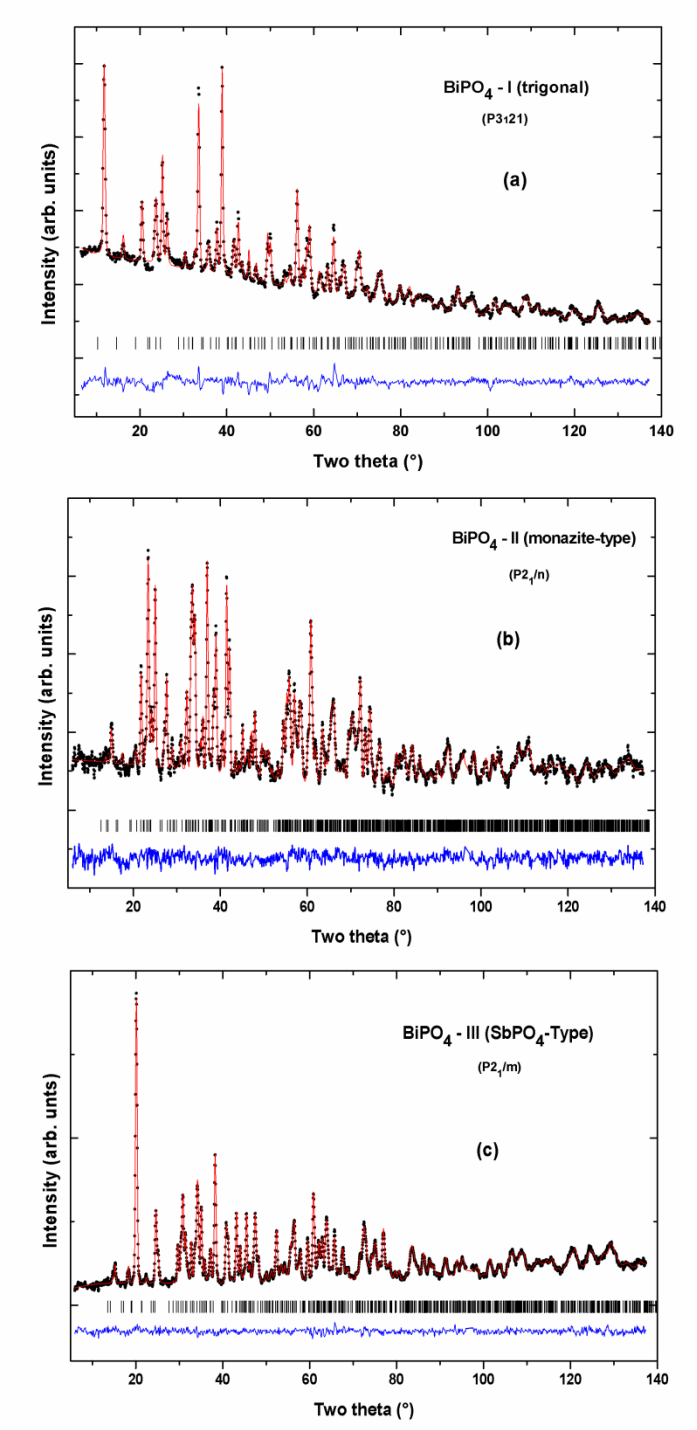

Fig. 2: Rietveld refinement plots of powder neutron diffraction data of $BiPO_4$ phases, (a). Trigonal (I), (b). Monazite-type (II) and (c). $SbPO_4$-type (III). ($\lambda = 1.249$ Å).

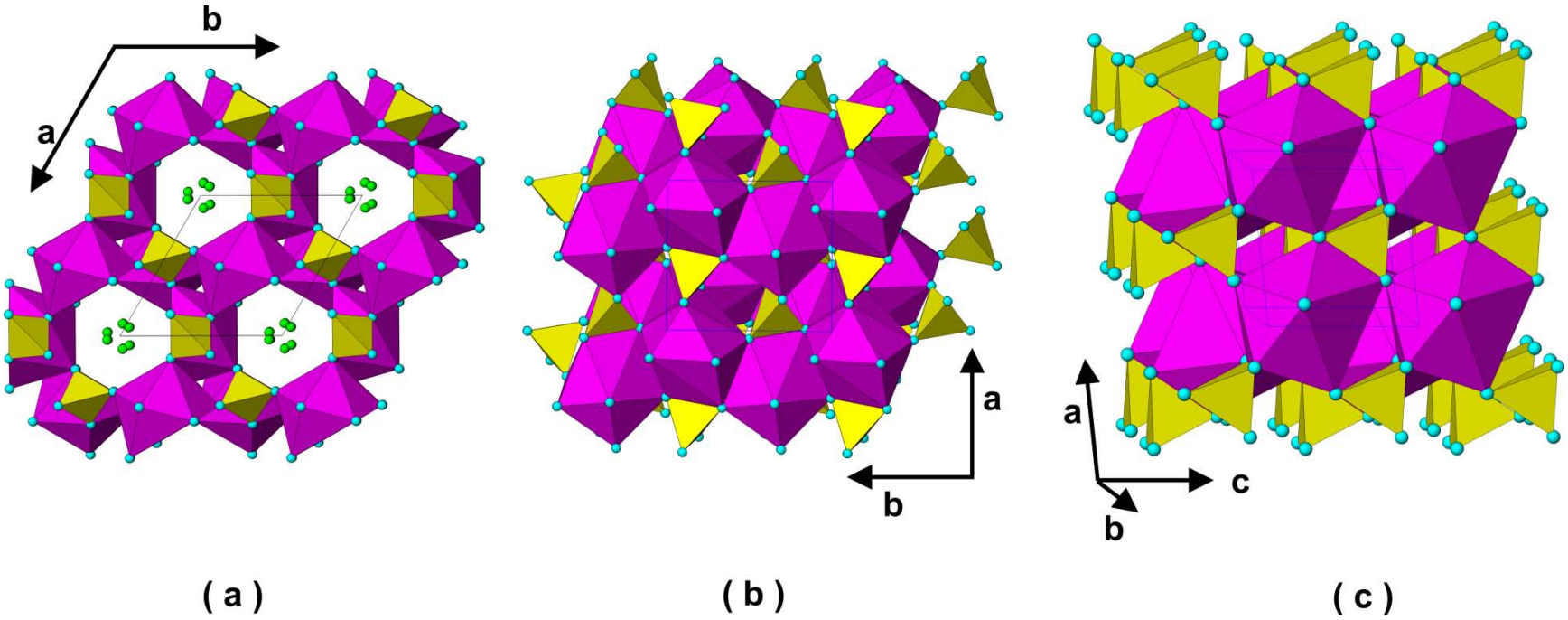

Fig. 3: Crystal structure of $BiPO_4$ phases, (a). Trigonal (I), (b). Monazite-type (II) and (c). $SbPO_4$-type (III). (BiO_8 (in a and c), BiO_9 (in b) and PO_4 units are shown). (isolated spheres are O3(of water molecules in $BiPO_4$-I).

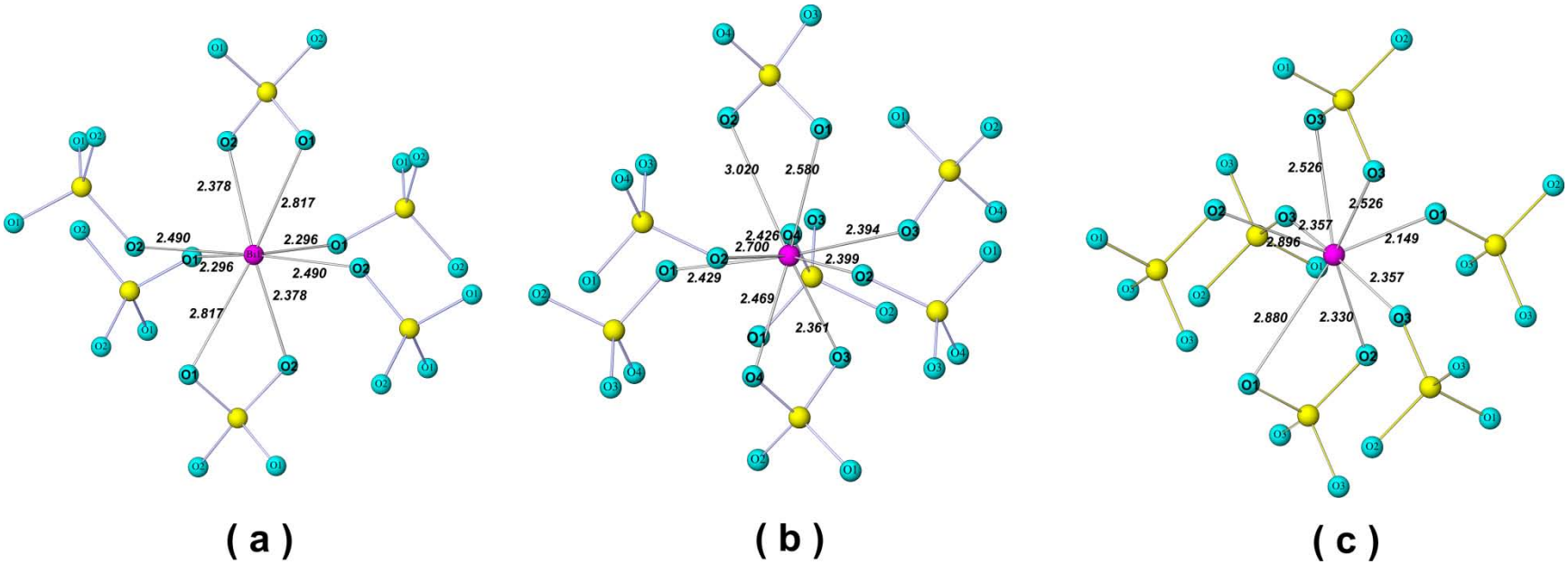

Fig. 4: Typical coordination around Bi^{3+} in $BiPO_4$ phases, (a). Trigonal (I), (b). Monazite type (II) and (c). $SbPO_4$ type (III)

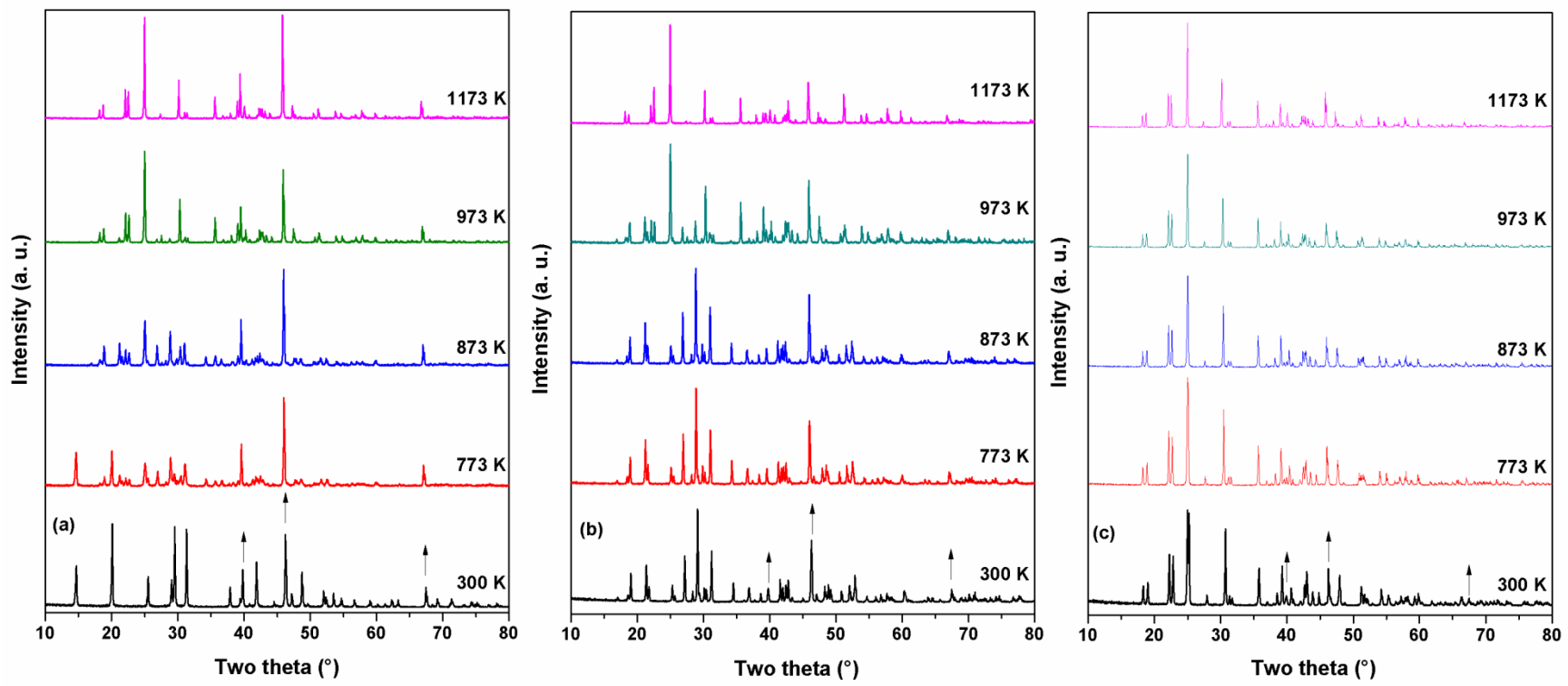

Fig. 5: Powder XRD patterns of $BiPO_4$ phases at representative temperatures. (a). Trigonal (I), (b). Monazite-type (II) and (c). $SbPO_4$-type (III) (↑ indicate platinum sample holder base peaks)

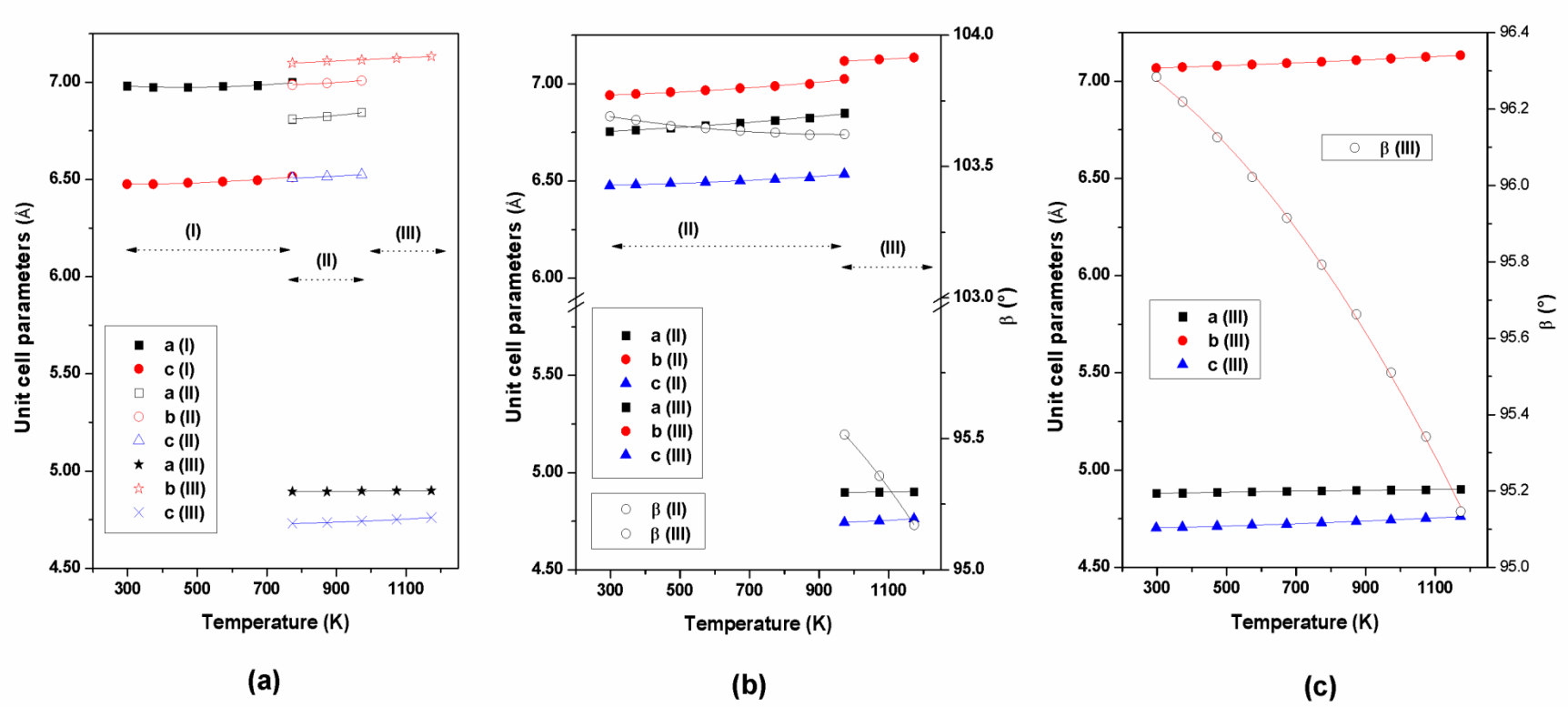

Fig. 6: Variation of unit cell parameters of $BiPO_4$ with temperature. (a). Trigonal (I), (b). Monazite-type (II) and (c). $SbPO_4$-type (III).

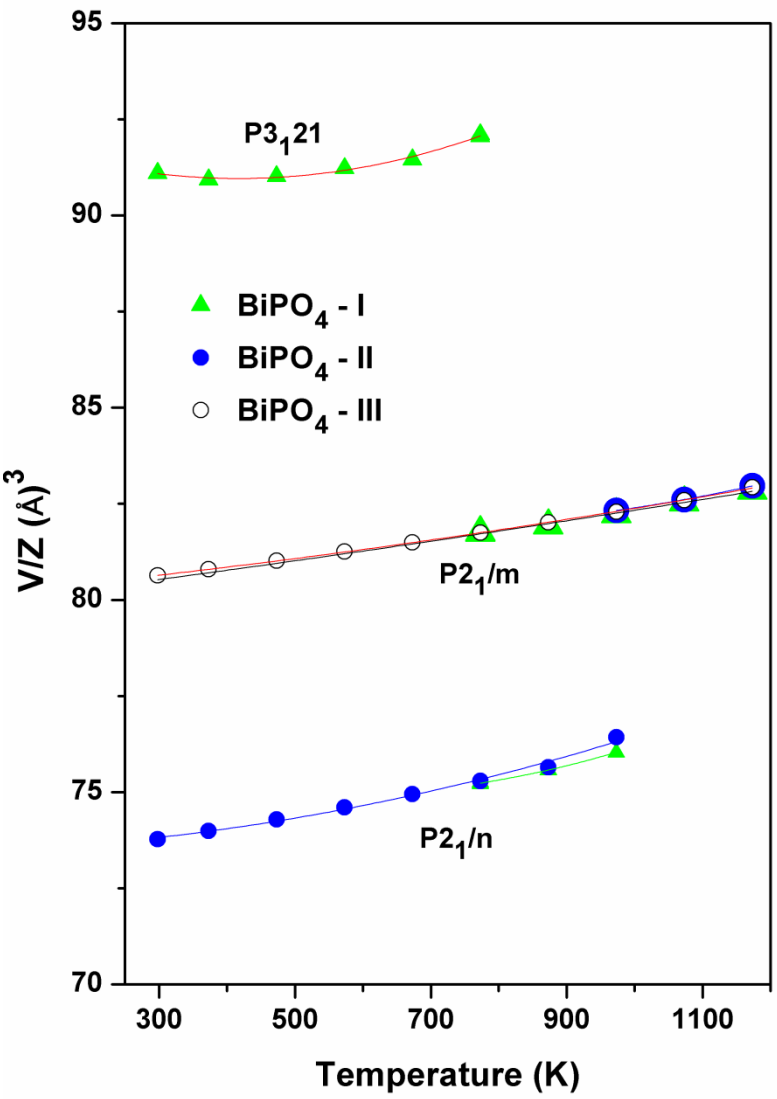

Fig. 7: Variation of molar volume of $BiPO_4$ phases with temperature.

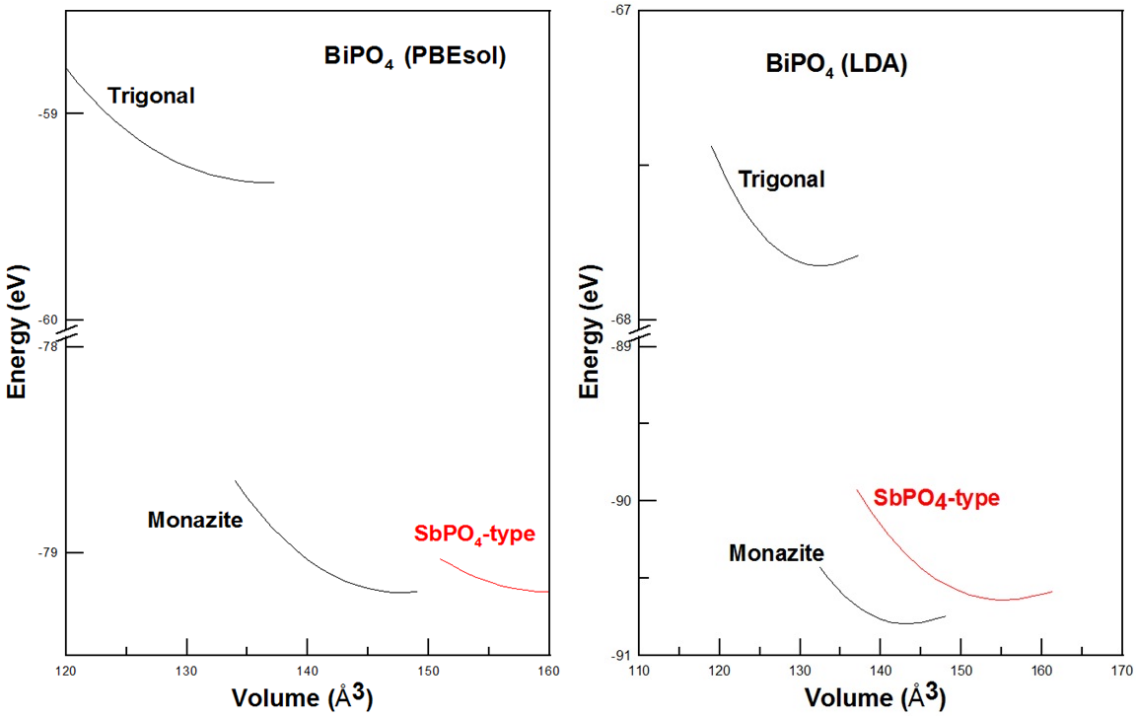

Fig. 8: Total energy as calculated by LDA and PBESol approach.

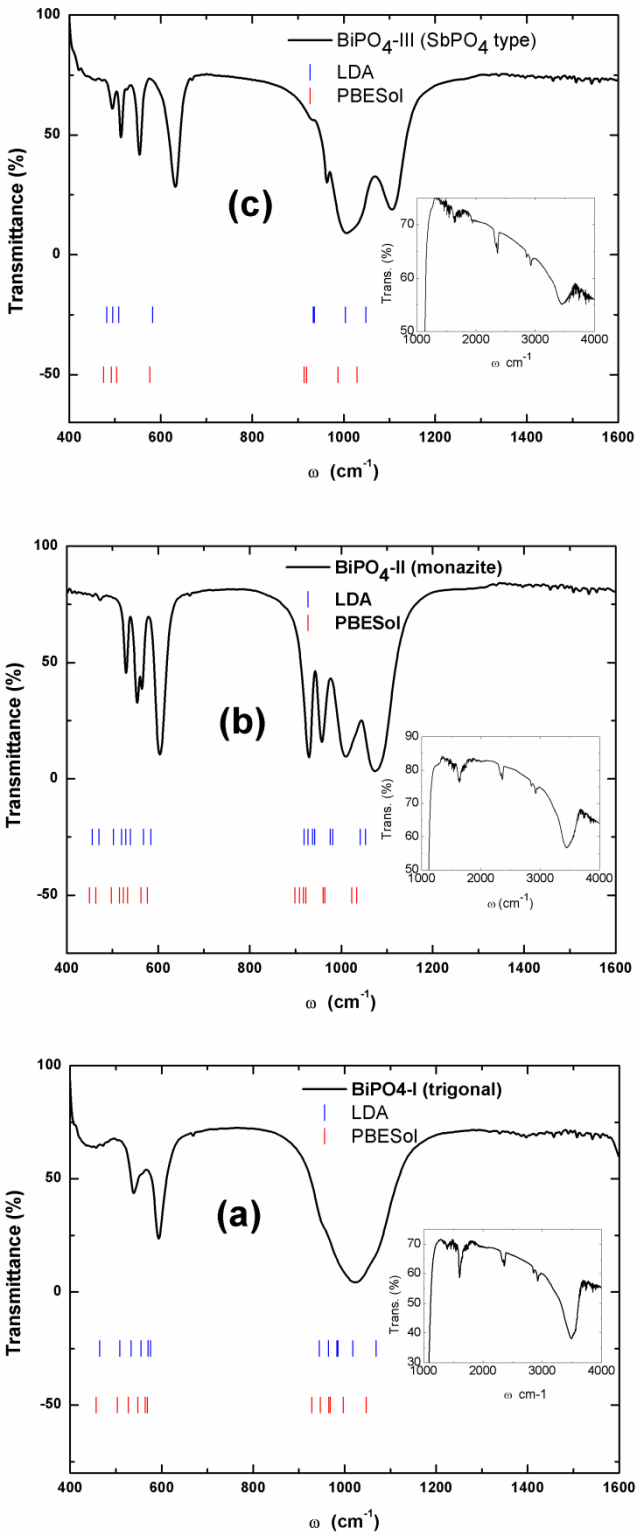

Fig. 9: Typical FTIR spectra of $BiPO_4$ phases. (a). Trigonal (I), (b). Monazite-type (II) and (c). $SbPO_4$-type (III). Vertical ticks indicate the calculated frequencies.

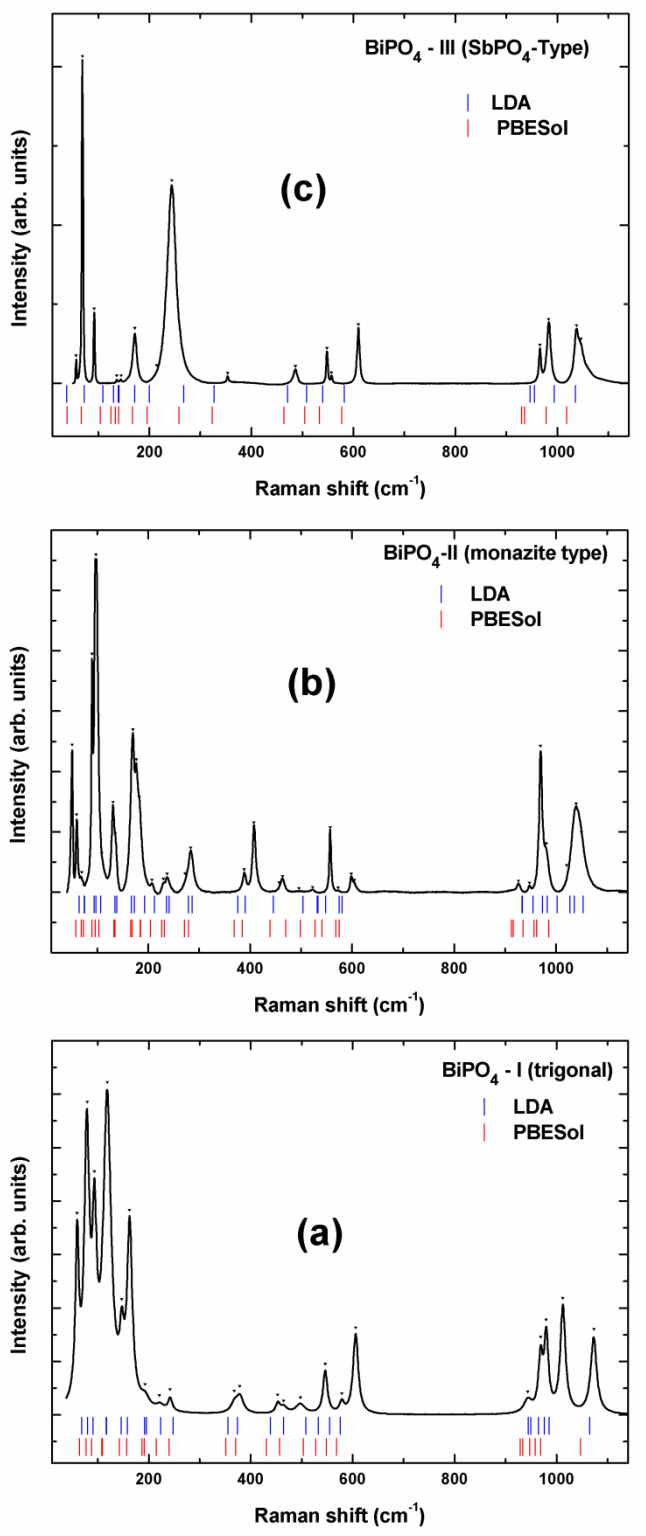

Fig. 10: Typical Raman spectra of $BiPO_4$ phases. (a). Trigonal (I), (b). Monazite-type (II) and (c). $SbPO_4$-type (III). Vertical ticks indicate the calculated frequencies.

Experimental and theoretical investigations on polymorphism and metastability of $BiPO_4$

S. N. Achary[1*], D. Errandonea [2], A. Muñoz[3], P. Rodríguez-Hernández[3], F. J. Manjón[4], P. S. R. Krishna [5], S. J. Patwe[1], V. Grover[1] and A. K. Tyagi [1]

[1]Chemistry Division, Bhabha Atomic Research Centre, Mumbai 400085, India
[2]MALTA Consolider Team, Departamento de Física Aplicada-ICMUV, Universitad de Valencia, Edificio de Investigación, c/Dr. Moliner 50, Burjassot, 46100 Valencia, Spain
[3]Departamento de Física Fundamental II, Instituto de Materiales y Nanotecnología, MALTA Consolider Team, Universidad de La Laguna, La Laguna 38205, Tenerife, Spain
[4] Instituto de Diseño para la Fabricación y Producción Automatizada, MALTA Consolider Team, Universitat Politècnica de València, 46022 València, Spain
[5]Solid State Physics Division, Bhabha Atomic Research Centre, Mumbai 400085, India

Supplementary information

Table-1. Refined structural parameters of $BiPO_4$-I at different temperatures. (from powder XRD data) .

a. Trigonal ($P3_121$) phase.

b. Trigonal ($P3_121$), Monazite type ($P2_1/n$) and $SbPO_4$-type ($P2_1/m$) coexisting phases (at 773 K).

c. Monazite type ($P2_1/n$) and $SbPO_4$-type ($P2_1/m$) coexisting phases (at 873 K).

d. $SbPO_4$-type ($P2_1/m$) phase

Table-2. Refined structural parameters of $BiPO_4$-II (Monazite-type) at different temperatures. (from powder XRD data)

a. Monazite type ($P2_1/n$) phases.

b. $SbPO_4$-type ($P2_1/m$) phase.

Table-3. Refined structural parameters of $BiPO_4$-III ($SbPO_4$ type) at different temperatures. (from powder XRD data)

d. $SbPO_4$-type ($P2_1/m$) phase

BiPO4-I				
Temp	873 K	973 K	1073	1173
a (Å) b (Å) c (Å) β (°) V $(Å)^3$	4.8930(5) 7.1088(8) 4.7342(5) 95.653(9) 163.87(3)	4.8964(2) 7.1154(3) 4.7421(2) 95.503(3) 164.46(1)	4.8985(1) 7.1238(2) 4.7510(1) 95.341(3) 165.07(1)	4.8993(2) 7.1325(2) 4.7605(2) 95.140(3) 165.68(1)
Bi 2e (x 1/4 z)	0.1452(9) 0.25000 0.1668(9)	0.1505(6) 0.2500 0.1650(6)	0.1506(6) 0.2500 0.1659(6)	0.1506(7) 0.2500 0.1638(7)
P 2e (x 3/4 z)	0.3739(9) 0.7500 0.3089(10)	0.3705(9) 0.7500 0.3106(9)	0.3686(9) 0.7500 0.3078(10)	0.3678(9) 0.7500 0.3098(10)
O1 2e (x 3/4 z)	0.674(1) 0.750 0.230(2)	0.674(1) 0.7500 0.241(2)	0.671(1) 0.750 0.234(2)	0.671(1) 0.750 0.238(2)
O2 2e (x 1/4 z)	0.618(2) 0.250 0.363(1)	0.6114(15) 0.25000 0.3617(10)	0.619(2) 0.250 0.365(1)	0.622(2) 0.250 0.364(1)
O3 4f (x y z)	0.203(5) 0.581(1) 0.202(6)	0.197(3) 0.591(1) 0.179(3)	0.201(3) 0.582(2) 0.194(4)	0.204(3) 0.5824(9) 0.193(4)
B_{ov} $(Å)^2$	1.9(2)	1.48(8)	3.63(11)	3.63(12)
Rp, Rwp, $\chi 2$	15.7, 22.0, 1.46	18.6, 24.8, 1.85	18.3, 24.6, 1.88	18.4, 24.8, 1.87
RB, RF	7.73, 6.80	8.63, 6.41	9.83, 8.40	13.4, 9.79
Bi-O1 (Å) Bi-O1 Bi-O2 Bi-O2 Bi-O3 Bi-O3 Bi-O3 Bi-O3	2.155(9) 2.905(9) 2.827(9 2.408(9) 2.3731(8) 2.610(22) 2.610(22) 2.373(8)	2.183(8) 2.865(8) 2.883(8) 2.358(7) 2.432(7) 2.513(13) 2.513(12) 2.432(7)	2.164(8) 2.904(8) 2.852(8) 2.400(8) 2.382(7) 2.602(15) 2.602(15) 2.382(7)	2.172(8) 2.905(8) 2.839(8) 2.418(8) 2.388(7) 2.608(15) 2.608(15) 2.388(7)
$<Bi-O>_8$ (Å)	2.532	2.522	2.536	2.541
Distt.	87.0×10^{-4}	79.7×10^{-4}	87.1×10^{-4}	82.9×10^{-4}
P-O1 (Å) P-O2 P-O3 P-O3	1.550(8) 1.548(7) 1.522(16) 1.522(16)	1.552(7) 1.548(6) 1.517(11) 1.517(11)	1.552(7) 1.550(7) 1.520(11) 1.520(11)	1.553(7) 1.548(7) 1.517(11) 1.517(11)
<P-O> (Å)	1.536	1.534	1.536	1.534
Distt.	0.761×10^{-4}	1.13×10^{-4}	1.00×10^{-4}	1.17×10^{-4}

Table-2. Refined structural parameters of BiPO4-II (Monazite type) at different temperatures. (As observed from powder XRD data)

a. Monazite type

	HT	HT_002	HT_003	HT2	HT2_002	HT2_003	HT2_004	HT2_005
Temp	298 K	373 K	473 K	573 K	673 K	773 K	873 K	973 K
Bi-O1 (Å)	2.568(11)	2.571(11)	2.573(11)	2.555(11)	2.566(11)	2.566(11)	2.610(12)	2.618
Bi-O1	2.481(9))	2.462(9)	2.458(9)	2.483(10)	2.475(10)	2.484(10)	2.428(11)	2.437
Bi-O2	3.052(11)	3.104(11)	3.109(11)	3.102(12)	3.082(12)	3.075(12)	3.076(12)	3.088
Bi-O2	2.396(9)	2.444(9)	2.428(9)	2.476(9)	2.481(9)	2.492(9)	2.495(10)	2.504
Bi-O2	2.679(10)	2.662(11)	2.663(11)	2.652(11)	2.679(11)	2.706(11)	2.717(12)	2.727
Bi-O3	2.314(9)	2.341(9)	2.307(9)	2.330(9)	2.320(9)	2.350(10)	2.320(10)	2.328
Bi-O3	2.507(11)	2.479(11)	2.523(11)	2.540(11)	2.543(11)	2.518(11)	2.566(12)	2.575
Bi-O4	2.516(12)	2.574(12)	2.608(12)	2.584(12)	2.665(12)	2.674(12)	2.688(12)	2.699
Bi-O4	2.445(10)	2.421(10)	2.413(9)	2.422(10)	2.372(9)	2.388(9)	2.390(10)	2.398)
$<Bi\text{-}O>_9$ (Å)	2.551	2.562	2.565	2.572	2.576	2.584	2.588	2.597
Distt.	62.7×10^{-4}	68.4×10^{-4}	72.5×10^{-4}	65.1×10^{-4}	67.3×10^{-4}	63.4×10^{-4}	68.2×10^{-4}	68.3×10^{-4}
P-O1 (Å)	1.541(10)	1.536(10)	1.537(10)	1.537(11)	1.537(11)	1.5361(107)	1.539(12)	1.544
P-O2	1.556(11)	1.553(11)	1.553(11)	1.551(11)	1.551(11)	1.5520(115)	1.556(12)	1.561
P-O3	1.529(8)	1.523(8)	1.528(8)	1.523(8)	1.520(8)	1.5227(84)	1.525(9)	1.530
P-O4	1.497(12)	1.494(12)	1.498(12)	1.493(12)	1.494(12)	1.4964(112)	1.496(12)	1.501
$<P\text{-}O>_4$ (Å)	1.531	1.527	1.529	1.526	1.525	1.527	1.529	1.534
Distt.	1.98×10^{-4}	2.00×10^{-4}	1.73×10^{-4}	1.94×10^{-4}	1.93×10^{-4}	1.78×10^{-4}	2.03×10^{-4}	2.06×10^{-4}

b. $SbPO_4$- type

		HT2_005 (R)	HT2_006 (R)	HT2_007 (R) e
Temp		973 K	1073 K	1173 K
a (Å) b (Å) c (Å) β (°) V $(Å)^3$		4.8991(1) 7.1173(2) 4.7441(1) 95.514(2) 164.653(8)	4.9004(2) 7.1257(2) 4.7523(2) 95.358(3) 165.219(9)	4.9022(2) 7.1344(3) 4.7621(3) 95.171(5) 165.876(14)
Bi	2e	0.1477(6) 0.2500 0.1638(6)	0.1499(6) 0.2500 0.1650(6)	0.1463(9) 0.2500 0.1638(9) 1.9141
P	2e	0.3680(10) 0.7500 0.3139(9)	0.3691(9) 0.7500 0.3094(10)	0.3603(9) 0.7500 0.3117(10) 0.2912
O1	2e	0.669(1) 0.750 0.240(2)	0.671(1) 0.750 0.237(2)	0.663(1) 0.750 0.237(2) 4.3468
O2	2e	0.615(2) 0.250 0.360(1)	0.618(2) 0.250 0.364(1)	0.619(2) 0.250 0.361(1) 4.3468
O3	4f	0.229(3) 0.579(1) 0.182(4)	0.208(3) 0.583(1) 0.188(4)	0.193(5) 0.581(1) 0.205(6) 4.3468
Bov		-0.57(8)	1.7(1)	
Rp, Rwp, $\chi 2$		20.3, 25.8, 2.69	22.3, 27.1, 2.93	28.2, 34.8, 4.36
RB, RF		20.9, 10.3	19.9, 11.3	30.8 , 18.6
Bi - O1 (Å) Bi - O1 Bi - O2 Bi - O2 Bi - O3 Bi - O3 Bi - O3 Bi - O3		2.193(8) 2.884(8) 2.853(8) 2.389(8) 2.373(6) 2.646(14) 2.646(14) 2.373(6)	2.175(8) 2.895(8) 2.856(8) 2.396(8) 2.388(7) 2.601(14) 2.601(15) 2.388(7)	2.200(9) 2.922(9) 2.829(9) 2.421(9) 2.380(8) 2.603(23) 2.603(23) 2.380(8)
<Bi-O> (Å)		2.545	2.537	2.542
Distt.		84.5×10^{-4}\	84.2×10^{-4}	81.0×10^{-4}
P - O1 (Å) P - O2 P - O3 P - O3		1.547(8) 1.540(6) 1.504(11) 1.504(11)	1.5513(73) 1.5474(67) 1.5151(111) 1.5151(111)	1.5565(77) 1.5518(67) 1.5191(162) 1.5191(162)
<P-O> (Å)		1.524	1.532	1.537
Distt.		1.70×10^{-4}	1.26×10^{-4}	1.31×10^{-4}

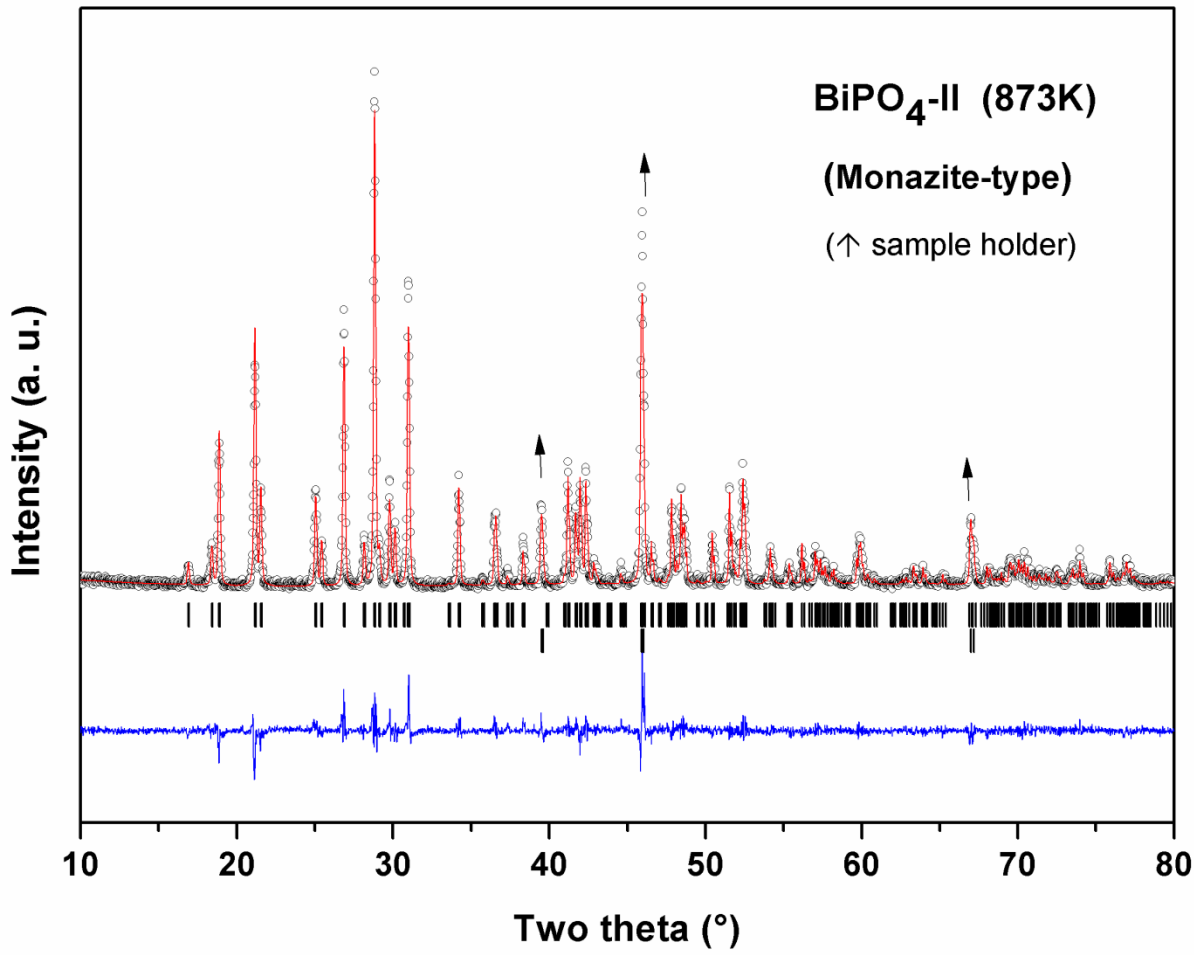

Fig.4. Rietveld refinement plot of the powder XRD data of $BiPO_4$-II at 873 K. (only monazite -type phase is observed). Arrows indicate reflections due to sample holder).

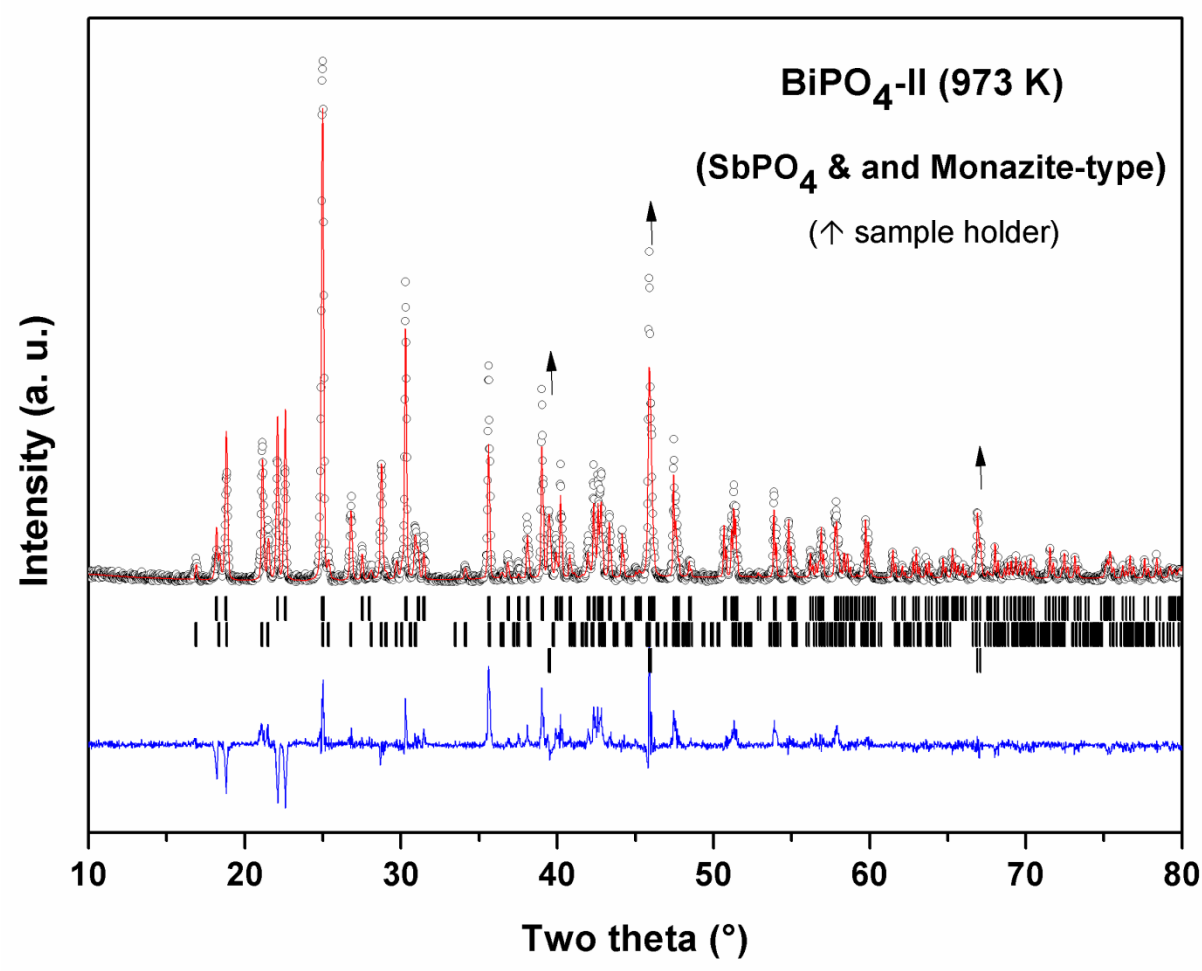

Fig.5. Rietveld refinement plot of the powder XRD data of $BiPO_4$-II at 973 K. (coexistence of monazite and $SbPO_4$-type phases are indicated by vertical ticks (from top to bottom). Arrows indicate reflections due to sample holder).

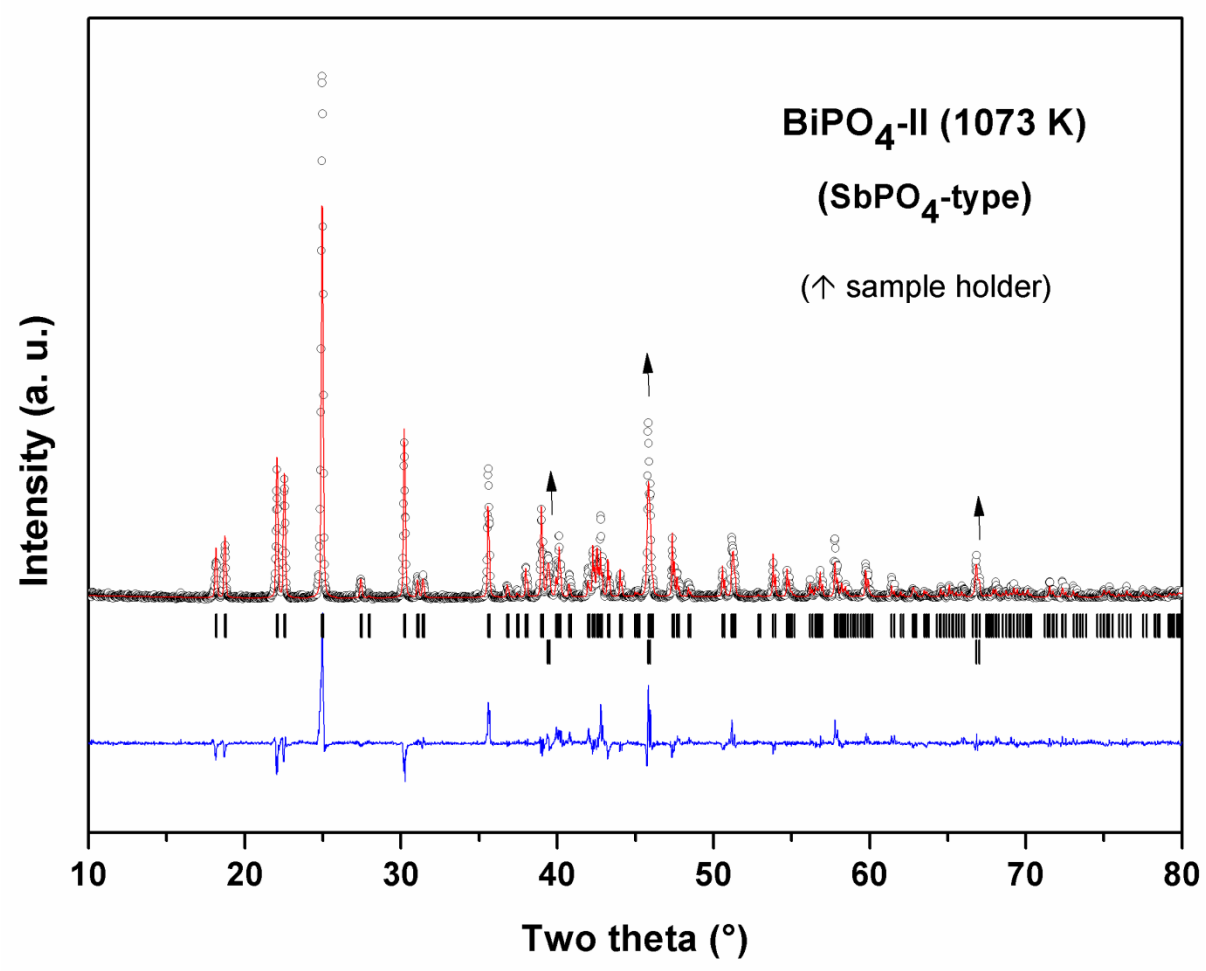

Fig.6. Rietveld refinement plot of the powder XRD data of $BiPO_4$-II at 1073 K. (Only $SbPO_4$-type phase is observed). Arrows indicate reflections due to sample holder)

Table-3. Refined structural parameters of BiPO4-III ($SbPO_4$ type) at different temperatures. (As observed from powder XRD data)

	HT	002	003	004	005	006	007	008	009	010
Temp	298	373	473	573	673	773	873	973	1073	1173
a (Å)	4.8804(1)	4.8828(1)	4.8857(1)	4.8884(1)	4.8912(1)	4.8936(1)	4.8959(1)	4.8980(1)	4.8997(1)	4.9015(1)
b (Å)	7.0684(2)	7.0729(2)	7.0797(2)	7.0867(2)	7.0935(2)	7.1011(2)	7.10897(18)	7.1169(2)	7.1252(2)	7.1346(2)
c (Å)	4.7033(1)	4.7067(1)	4.7116(1)	4.7170(1)	4.7228(1)	4.7290(1)	4.73601(12)	4.7434(1)	4.7520(1)	4.7618(1)
β (°)	96.285(3)	96.219(3)	96.126(2)	96.022(2)	95.915(2)	95.792(2)	95.662(2)	95.510(2)	95.342(2)	95.146(2)
V $(Å)^3$	161.272(8)	161.591(8)	162.039(7)	162.508(7)	162.985(7)	163.496(7)	164.032(7)	164.583(7)	165.177(7)	165.849(7)
BI	0.1433(4)	0.1437(4)	0.1444(4)	0.1462(4)	0.1458(4)	0.1477(4)	0.1484(5)	0.1491(5)	0.1495(5)	0.1496(6)
x y z Biso $Å^2$	0.2500	0.2500	0.2500	0.2500	0.2500	0.2500	0.2500	0.2500	0.2500	0.2500
	0.1681(4)	0.1673(4)	0.1664(4)	0.1671(4)	0.1662(4)	0.1658(4)	0.1653(4)	0.1652(5)	0.1645(5)	0.1648(6)
	0.33(5)	0.21(5)	0.28(5)	0.34(5)	0.57(6)	0.72(6)	0.93(6)	1.25(6)	1.60(7)	1.91(8)
P	0.3751(9)	0.3741(9)	0.3724(9)	0.3697(9)	0.3717(9)	0.3699(9)	0.3696(9)	0.3691(9)	0.3689(9)	0.3683(9)
	0.7500	0.7500	0.7500	0.7500	0.7500	0.7500	0.7500	0.7500	0.7500	0.7500
	0.3092(9)	0.3067(9)	0.3065(9)	0.3088(9)	0.3090(9)	0.3094(9)	0.3094(9)	0.3081(9)	0.3082(9)	0.3086(10)
	0.32	0.32	0.32	0.32	0.32	0.32	0.320	0.32	0.2(3)	0.3(4)
O1	0.676(2)	0.673(2)	0.674(2)	0.672(2)	0.672(2)	0.671(2)	0.671(2)	0.672(2)	0.670(2)	0.670(2)
	0.750	0.7500	0.750	0.750	0.7500	0.750	0.750	0.750	0.750	0.750
	0.234(4)	0.225(4)	0.232(4)	0.238(4)	0.231(4)	0.235(5)	0.236(5)	0.238(5)	0.234(5)	0.235(6)
	1.0(3)	0.7(3)	0.8(3)	1.0(3)	1.0(3)	1.6(4)	2.2(4)	2.0(4)	3.1(4)	4.3(5)
O2	0.603(4)	0.601(4)	0.608(4)	0.611(4)	0.611(4)	0.609(5)	0.611(5)	0.617(5)	0.619(5)	0.622(7)
	0.250	0.2500	0.2500	0.2500	0.2500	0.250	0.250	0.250	0.250	0.250
	0.361(1)	0.364(1)	0.365(1)	0.363(1)	0.363(1)	0.363(1	0.363(1)	0.365(1)	0.366(1)	0.365(1)
	1.0(3)	0.7(3)	0.8(3)	1.0(3)	1.0(3)	1.6(4)	2.2(4)	2.0(4)	3.1(4)	4.3(5)
O3	0.220(3)	0.220(3)	0.218(3)	0.217(3)	0.218(3)	0.212(3)	0.211(3)	0.212(3)	0.204(3)	0.202(4)
	0.578(1)	0.577(1)	0.577(1)	0.577(1)	0.577(1)	0.580(1)	0.578(1)	0.578(1)	0.581(2)	0.581(2)
	0.183(3)	0.184(3)	0.188(3)	0.188(3)	0.191(3)	0.186(3)	0.193(3)	0.194(3)	0.195(4)	0.199(4)
	1.0(3)	0.7(3)	0.8(3)	1.0(3)	1.0(3)	1.6(4)	2.2(4)	2.0(4)	3.1(4)	4.3(5)
Rp, Rwp	13.5, 19.0,	13.4, 18.6,	13.2, 18.7,	13.0,18.3,	13.6, 18.7,	13.4, 18.8,	13.5, 19.0,	13.6, 18.8,	14.4, 19.6,	15.7, 21.2,
$\chi 2$	1.60	1.54	1.56	1.51	1.58	1.60	1.63	1.61	1.74	1.90
RB, RF	5.97, 3.41	5.62, 3.35	5.98, 3.53	5.41, 3.52	5.48, 3.87	5.65, 3.90	5.43, 4.32	5.98, 4.90	6.52, 5.30	7.17, 6.06

Table-3. Refined structural parameters of $BiPO_4$-III ($SbPO_4$ type) at different temperatures. (As observed from powder XRD data)

	HT	002	003	004	005	006	007	008	009	010
Temp	298 K	373 K	473 K	573 K	673 K	773 K	873 K	973 K	1073 K	1173 K
Bi-O1 (Å)	2.172(18)	2.138(18)	2.161(18)	2.191(18)	2.160(18)	2.172(22)	2.173(22)	2.180(22)	2.164(22)	2.170(27)
Bi-O1	2.853(18)	2.903(18)	2.879(18)	2.853(18)	2.895(18)	2.883(23)	2.885(23)	2.882(23)	2.912(23)	2.915(27)
Bi-O2	2.881(18)	2.899(19)	2.874(19)	2.864(19)	2.864(19)	2.883(23)	2.878(23)	2.857(23)	2.852(23)	2.837(32)
Bi-O2	2.326(18)	2.322(18)	2.356(18)	2.361(18)	2.367(18)	2.353(22)	2.364(23)	2.394(23)	2.407(23)	2.424(32)
Bi-O3	2.351(9)	2.343(9)	2.343(9)	2.341(9)	2.345(9)	2.364(10)	2.355(10)	2.358(10)	2.378(12)	2.382(14)
Bi-O3	2.589(13)	2.598(13)	2.606(13)	2.616(13)	2.628(13)	2.595(13)	2.623(13)	2.636(13)	2.610(15)	2.623(18)
Bi-O3	2.589(13)	2.598(13)	2.606(13)	2.616(13)	2.628(13)	2.595(13)	2.623(13)	2.636(13)	2.610(15)	2.623(18)
Bi-O3	2.351(9)	2.343(9)	2.343(9)	2.341(9)	2.345(9)	2.364(10)	2.355(10)	2.358(10)	2.378(12))	2.382(15)
<P-O> (Å)	2.514	2.518	2.521	2.523	2.529	2.526	2.532	2.538	2.539	2.544
Distt.	92.3×10^{-4}	108.4×10^{-4}	95.8×10^{-4}	87.5×10^{-4}	97.0×10^{-4}	92.4×10^{-4}	93.8×10^{-4}	88.0×10^{-4}	88.7×10^{-4}	85.3×10^{-4}
P-O1 (Å)	1.549(11)	1.548(12)	1.548(11)	1.548(11)	1.548(11)	1.549(12)	1.551(12)	1.550(12)	1.548(13)	1.550(14)
P-O2	1.543(7)	1.544(6)	1.542(7)	1.543(7)	1.544(7)	1.544(7)	1.545(7)	1.547(7)	1.546(7)	1.549(7)
P-O3	1.516(11)	1.517(11)	1.514(11)	1.518(11)	1.517(11)	1.519(12)	1.521(12)	1.517(12)	1.519(13)	1.519(16)
P-O3	1.516(11)	1.517(11)	1.514(11)	1.518(11)	1.517(11)	1.519(12)	1.521(12)	1.517(12)	1.519(13)	1.519(16)
<P-O> Å)	1.531	1.531	1.530	1.532	1.532	1.533	1.534	1.533	1.533	1.534
Distt.	0.96×10^{-4}	0.89×10^{-4}	1.10×10^{-4}	0.86×10^{-4}	0.90×10^{-4}	0.82×10^{-4}	0.77×10^{-4}	1.08×10^{-4}	0.82×10^{-4}	1.00×10^{-4}

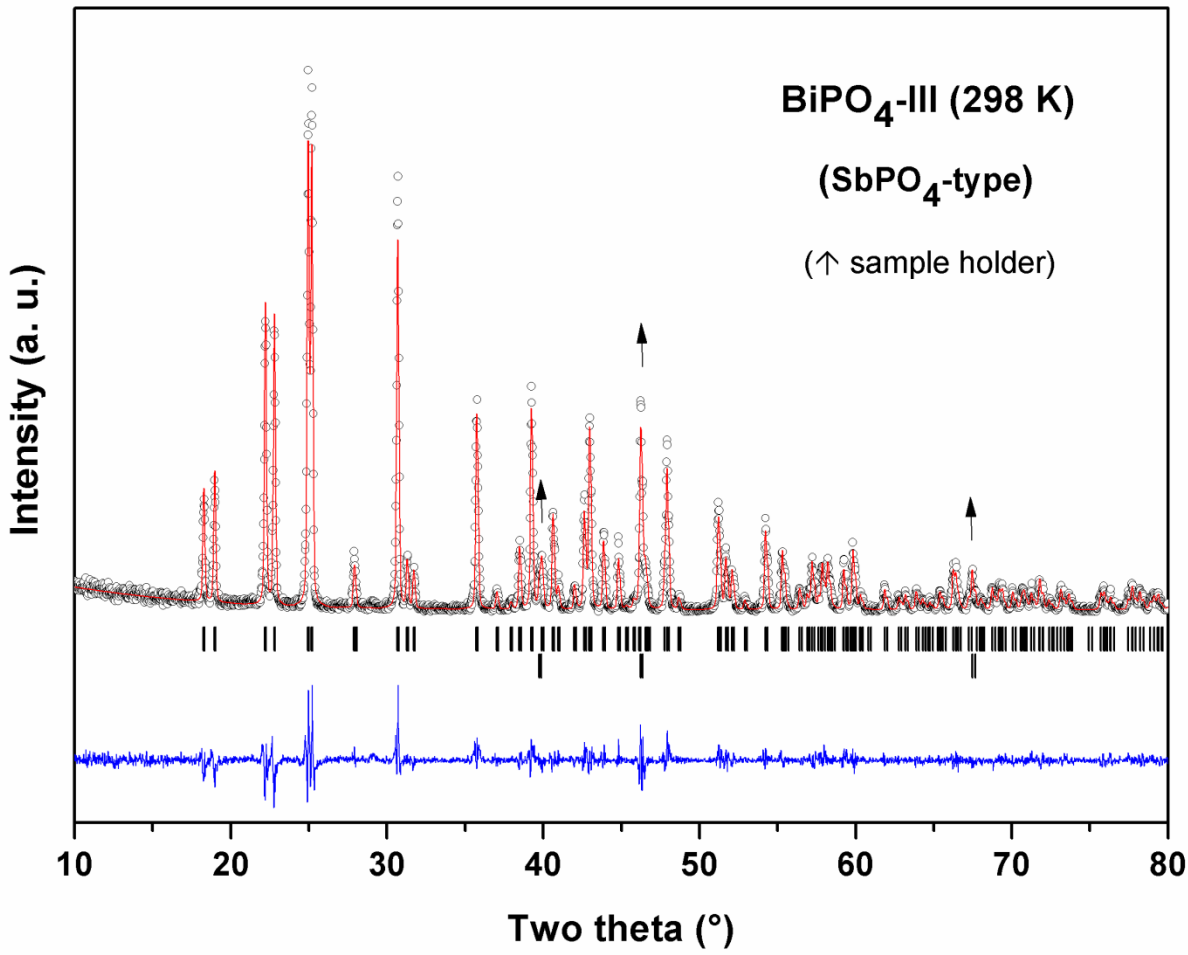

Fig.7. Rietveld refinement plot of the powder XRD data of $BiPO_4$-III at 298 K. (Only $SbPO_4$-type phases is observed). Arrows indicate reflections due to sample holder)

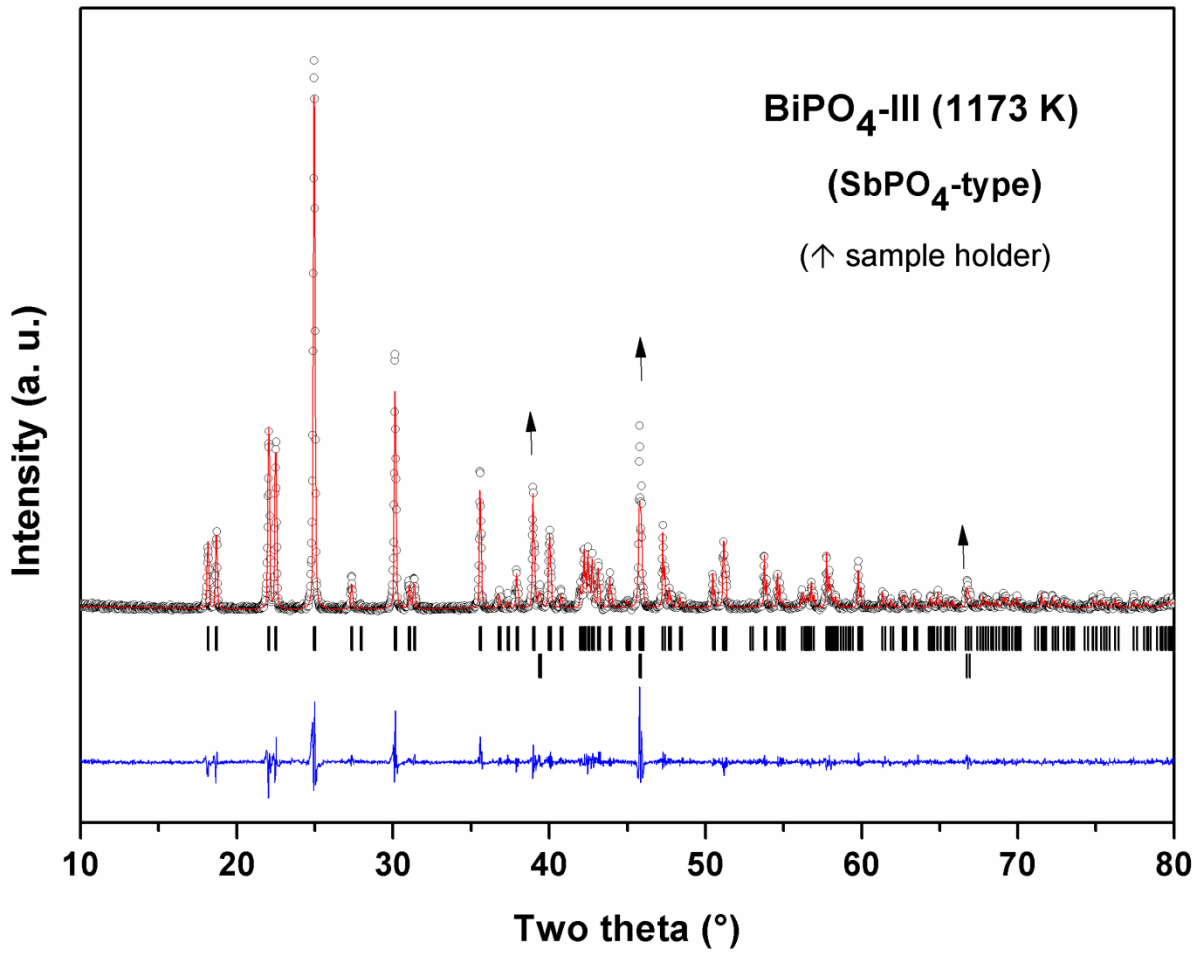

Fig.8. Rietveld refinement plot of the powder XRD data of $BiPO_4$-III at 1173 K. (Only $SbPO_4$-type phase is observed). Arrows indicate reflections due to sample holder)

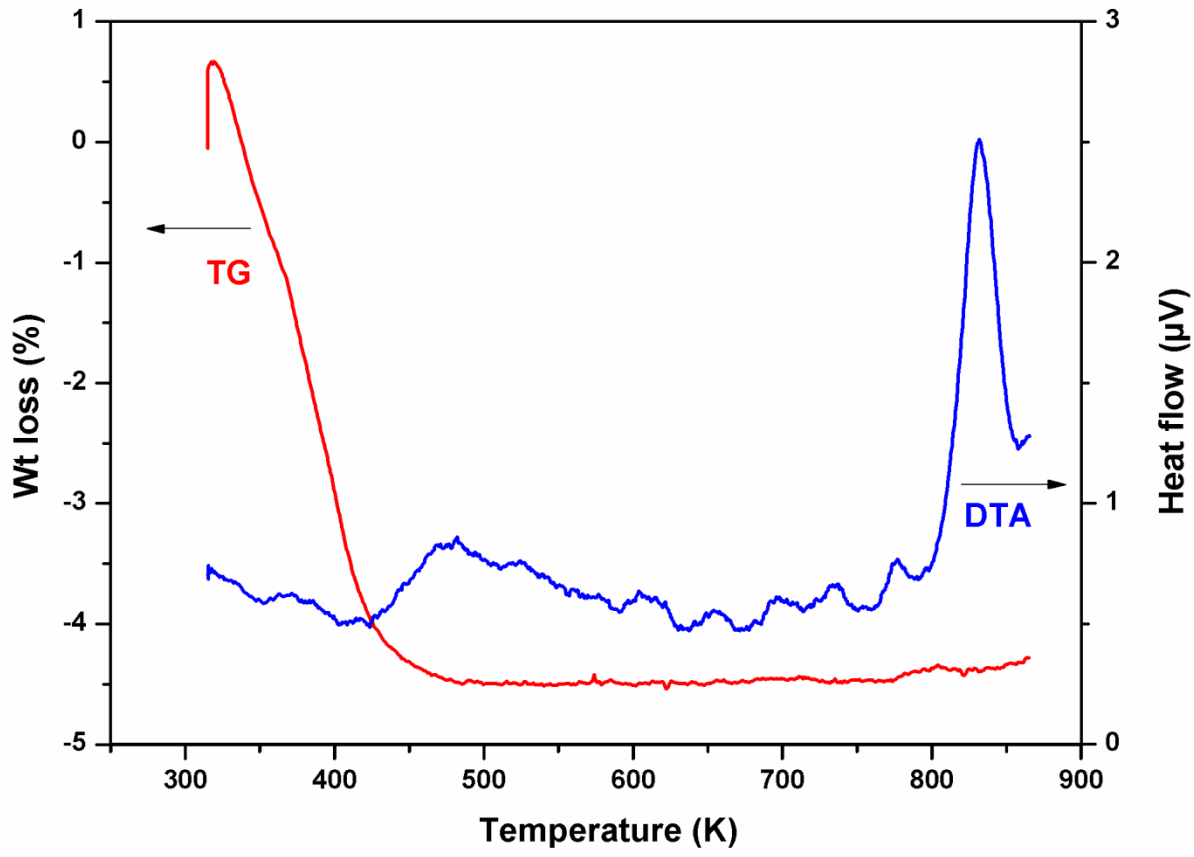

Fig.9. Typical TG-DTA traces of as prepared sample of hydrated trigonal $BiPO_4$ sample. (Sample was heated from 323 to 873 K at a rate of 10K/min).

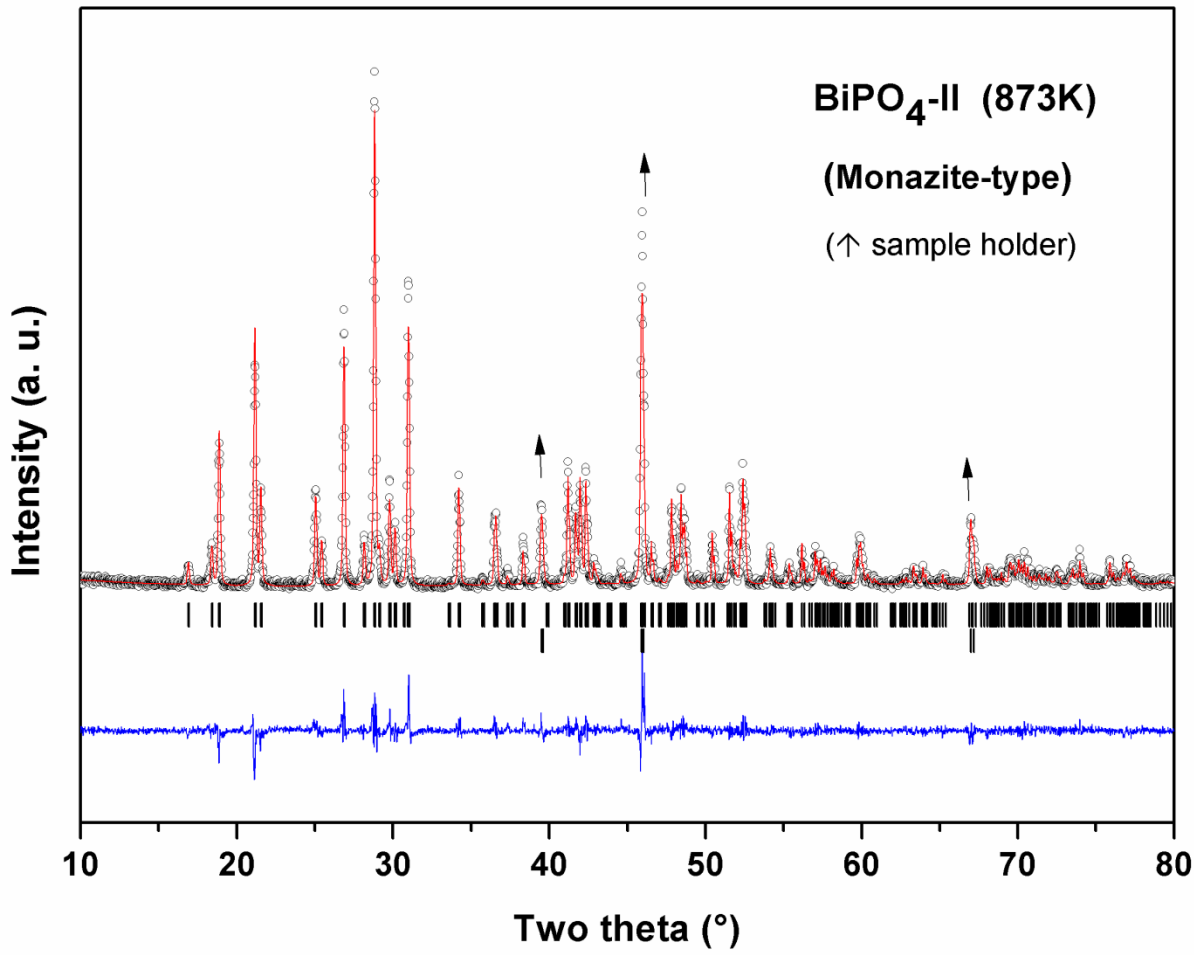

Fig.4. Rietveld refinement plot of the powder XRD data of $BiPO_4$-II at 873 K. (only monazite -type phase is observed). Arrows indicate reflections due to sample holder).

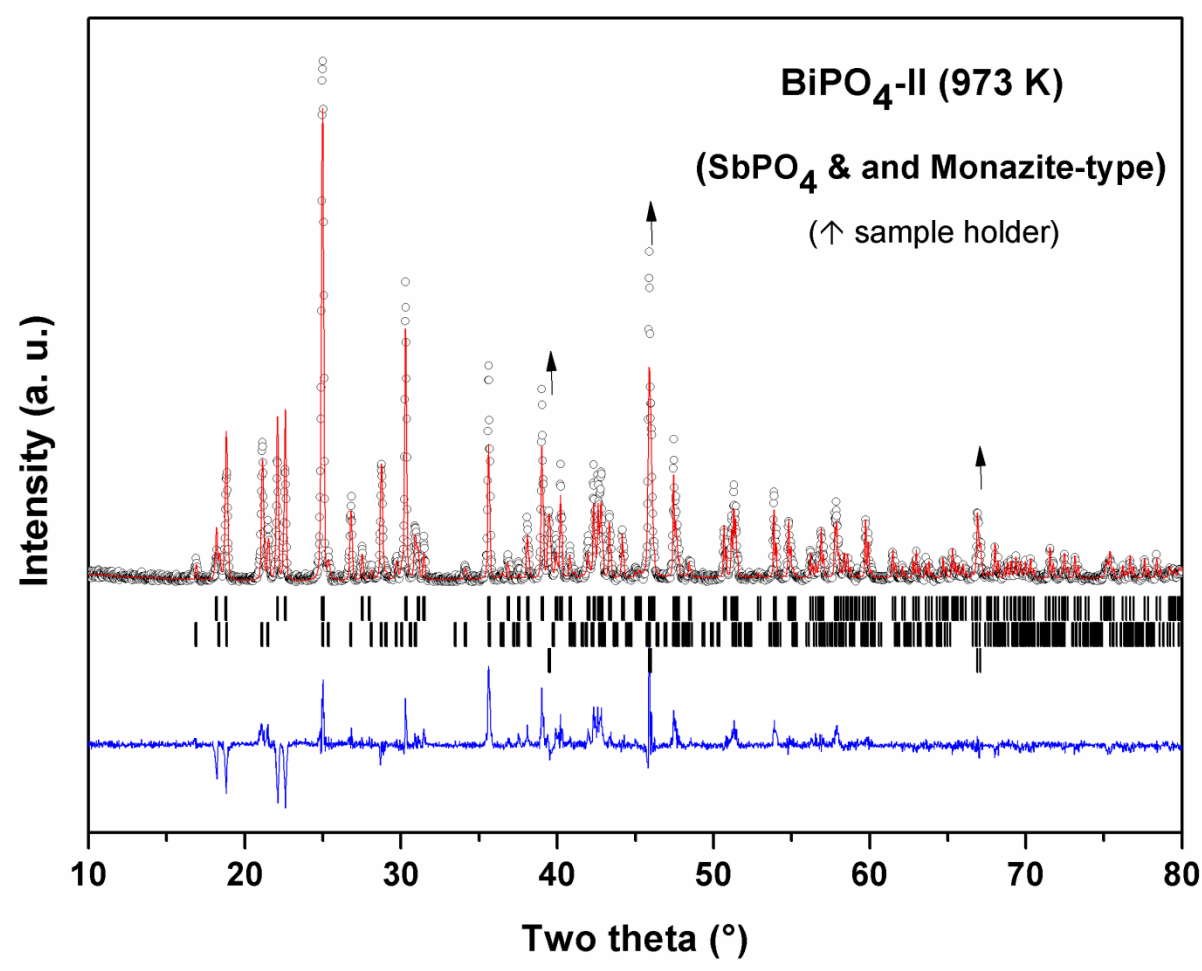

Fig.5. Rietveld refinement plot of the powder XRD data of $BiPO_4$-II at 973 K. (coexistence of monazite and $SbPO_4$-type phases are indicated by vertical ticks (from top to bottom). Arrows indicate reflections due to sample holder).

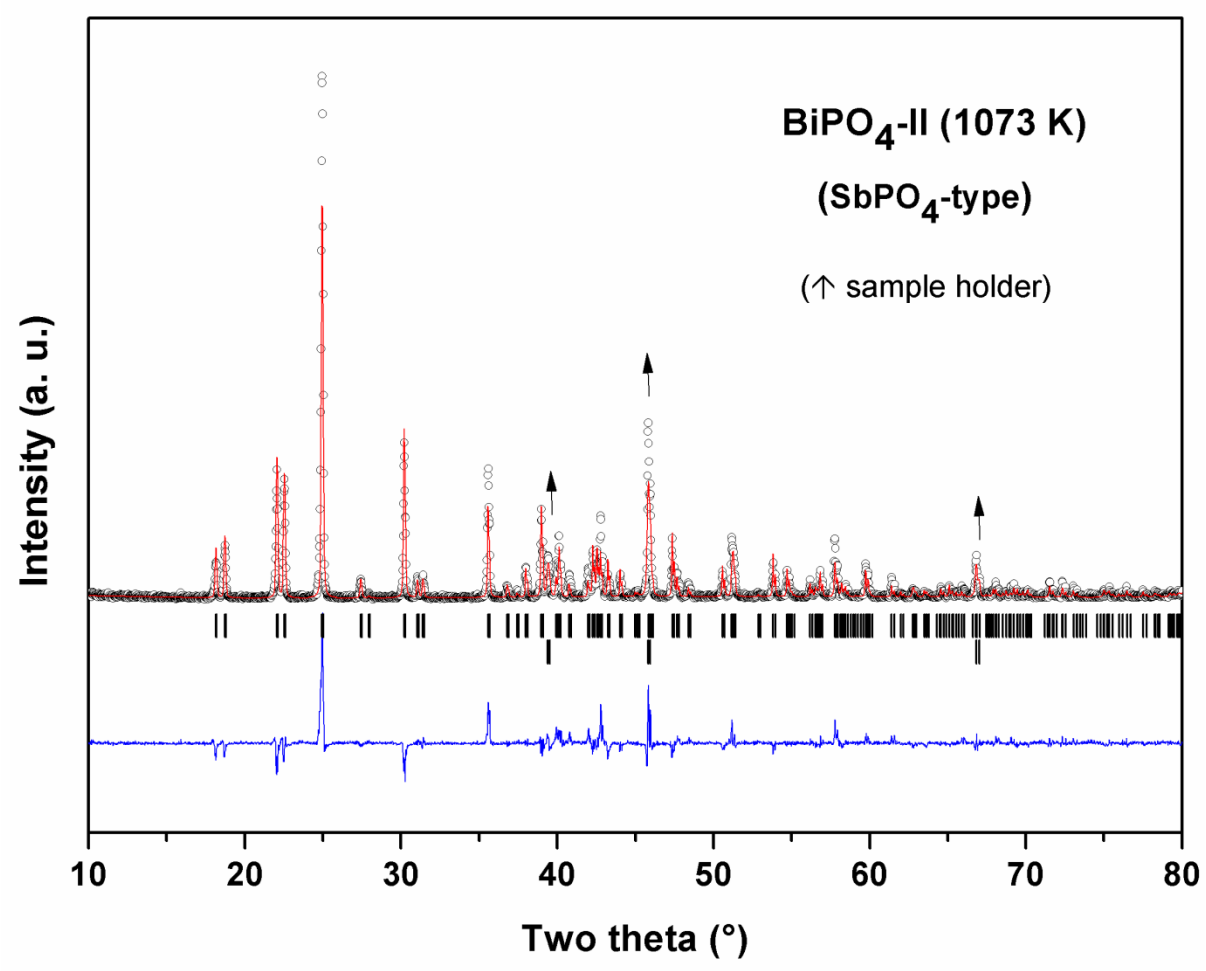

Fig.6. Rietveld refinement plot of the powder XRD data of $BiPO_4$-II at 1073 K. (Only $SbPO_4$-type phase is observed). Arrows indicate reflections due to sample holder)

Table-3. Refined structural parameters of BiPO4-III ($SbPO_4$ type) at different temperatures. (As observed from powder XRD data)

	HT	002	003	004	005	006	007	008	009	010
Temp	298	373	473	573	673	773	873	973	1073	1173
a (Å)	4.8804(1)	4.8828(1)	4.8857(1)	4.8884(1)	4.8912(1)	4.8936(1)	4.8959(1)	4.8980(1)	4.8997(1)	4.9015(1)
b (Å)	7.0684(2)	7.0729(2)	7.0797(2)	7.0867(2)	7.0935(2)	7.1011(2)	7.10897(18)	7.1169(2)	7.1252(2)	7.1346(2)
c (Å)	4.7033(1)	4.7067(1)	4.7116(1)	4.7170(1)	4.7228(1)	4.7290(1)	4.73601(12)	4.7434(1)	4.7520(1)	4.7618(1)
β (°)	96.285(3)	96.219(3)	96.126(2)	96.022(2)	95.915(2)	95.792(2)	95.662(2)	95.510(2)	95.342(2)	95.146(2)
V $(Å)^3$	161.272(8)	161.591(8)	162.039(7)	162.508(7)	162.985(7)	163.496(7)	164.032(7)	164.583(7)	165.177(7)	165.849(7)
BI	0.1433(4)	0.1437(4)	0.1444(4)	0.1462(4)	0.1458(4)	0.1477(4)	0.1484(5)	0.1491(5)	0.1495(5)	0.1496(6)
x y z Biso $Å^2$	0.2500	0.2500	0.2500	0.2500	0.2500	0.2500	0.2500	0.2500	0.2500	0.2500
	0.1681(4)	0.1673(4)	0.1664(4)	0.1671(4)	0.1662(4)	0.1658(4)	0.1653(4)	0.1652(5)	0.1645(5)	0.1648(6)
	0.33(5)	0.21(5)	0.28(5)	0.34(5)	0.57(6)	0.72(6)	0.93(6)	1.25(6)	1.60(7)	1.91(8)
P	0.3751(9)	0.3741(9)	0.3724(9)	0.3697(9)	0.3717(9)	0.3699(9)	0.3696(9)	0.3691(9)	0.3689(9)	0.3683(9)
	0.7500	0.7500	0.7500	0.7500	0.7500	0.7500	0.7500	0.7500	0.7500	0.7500
	0.3092(9)	0.3067(9)	0.3065(9)	0.3088(9)	0.3090(9)	0.3094(9)	0.3094(9)	0.3081(9)	0.3082(9)	0.3086(10)
	0.32	0.32	0.32	0.32	0.32	0.32	0.320	0.32	0.2(3)	0.3(4)
O1	0.676(2)	0.673(2)	0.674(2)	0.672(2)	0.672(2)	0.671(2)	0.671(2)	0.672(2)	0.670(2)	0.670(2)
	0.750	0.7500	0.750	0.750	0.7500	0.750	0.750	0.750	0.750	0.750
	0.234(4)	0.225(4)	0.232(4)	0.238(4)	0.231(4)	0.235(5)	0.236(5)	0.238(5)	0.234(5)	0.235(6)
	1.0(3)	0.7(3)	0.8(3)	1.0(3)	1.0(3)	1.6(4)	2.2(4)	2.0(4)	3.1(4)	4.3(5)
O2	0.603(4)	0.601(4)	0.608(4)	0.611(4)	0.611(4)	0.609(5)	0.611(5)	0.617(5)	0.619(5)	0.622(7)
	0.250	0.2500	0.2500	0.2500	0.2500	0.250	0.250	0.250	0.250	0.250
	0.361(1)	0.364(1)	0.365(1)	0.363(1)	0.363(1)	0.363(1	0.363(1)	0.365(1)	0.366(1)	0.365(1)
	1.0(3)	0.7(3)	0.8(3)	1.0(3)	1.0(3)	1.6(4)	2.2(4)	2.0(4)	3.1(4)	4.3(5)
O3	0.220(3)	0.220(3)	0.218(3)	0.217(3)	0.218(3)	0.212(3)	0.211(3)	0.212(3)	0.204(3)	0.202(4)
	0.578(1)	0.577(1)	0.577(1)	0.577(1)	0.577(1)	0.580(1)	0.578(1)	0.578(1)	0.581(2)	0.581(2)
	0.183(3)	0.184(3)	0.188(3)	0.188(3)	0.191(3)	0.186(3)	0.193(3)	0.194(3)	0.195(4)	0.199(4)
	1.0(3)	0.7(3)	0.8(3)	1.0(3)	1.0(3)	1.6(4)	2.2(4)	2.0(4)	3.1(4)	4.3(5)
Rp, Rwp	13.5, 19.0,	13.4, 18.6,	13.2, 18.7,	13.0,18.3,	13.6, 18.7,	13.4, 18.8,	13.5, 19.0,	13.6, 18.8,	14.4, 19.6,	15.7, 21.2,
$\chi 2$	1.60	1.54	1.56	1.51	1.58	1.60	1.63	1.61	1.74	1.90
RB, RF	5.97, 3.41	5.62, 3.35	5.98, 3.53	5.41, 3.52	5.48, 3.87	5.65, 3.90	5.43, 4.32	5.98, 4.90	6.52, 5.30	7.17, 6.06

Table-3. Refined structural parameters of $BiPO_4$-III ($SbPO_4$ type) at different temperatures. (As observed from powder XRD data)

	HT	002	003	004	005	006	007	008	009	010
Temp	298 K	373 K	473 K	573 K	673 K	773 K	873 K	973 K	1073 K	1173 K
Bi-O1 (Å)	2.172(18)	2.138(18)	2.161(18)	2.191(18)	2.160(18)	2.172(22)	2.173(22)	2.180(22)	2.164(22)	2.170(27)
Bi-O1	2.853(18)	2.903(18)	2.879(18)	2.853(18)	2.895(18)	2.883(23)	2.885(23)	2.882(23)	2.912(23)	2.915(27)
Bi-O2	2.881(18)	2.899(19)	2.874(19)	2.864(19)	2.864(19)	2.883(23)	2.878(23)	2.857(23)	2.852(23)	2.837(32)
Bi-O2	2.326(18)	2.322(18)	2.356(18)	2.361(18)	2.367(18)	2.353(22)	2.364(23)	2.394(23)	2.407(23)	2.424(32)
Bi-O3	2.351(9)	2.343(9)	2.343(9)	2.341(9)	2.345(9)	2.364(10)	2.355(10)	2.358(10)	2.378(12)	2.382(14)
Bi-O3	2.589(13)	2.598(13)	2.606(13)	2.616(13)	2.628(13)	2.595(13)	2.623(13)	2.636(13)	2.610(15)	2.623(18)
Bi-O3	2.589(13)	2.598(13)	2.606(13)	2.616(13)	2.628(13)	2.595(13)	2.623(13)	2.636(13)	2.610(15)	2.623(18)
Bi-O3	2.351(9)	2.343(9)	2.343(9)	2.341(9)	2.345(9)	2.364(10)	2.355(10)	2.358(10)	2.378(12))	2.382(15)
<P-O> (Å)	2.514	2.518	2.521	2.523	2.529	2.526	2.532	2.538	2.539	2.544
Distt.	92.3×10^{-4}	108.4×10^{-4}	95.8×10^{-4}	87.5×10^{-4}	97.0×10^{-4}	92.4×10^{-4}	93.8×10^{-4}	88.0×10^{-4}	88.7×10^{-4}	85.3×10^{-4}
P-O1 (Å)	1.549(11)	1.548(12)	1.548(11)	1.548(11)	1.548(11)	1.549(12)	1.551(12)	1.550(12)	1.548(13)	1.550(14)
P-O2	1.543(7)	1.544(6)	1.542(7)	1.543(7)	1.544(7)	1.544(7)	1.545(7)	1.547(7)	1.546(7)	1.549(7)
P-O3	1.516(11)	1.517(11)	1.514(11)	1.518(11)	1.517(11)	1.519(12)	1.521(12)	1.517(12)	1.519(13)	1.519(16)
P-O3	1.516(11)	1.517(11)	1.514(11)	1.518(11)	1.517(11)	1.519(12)	1.521(12)	1.517(12)	1.519(13)	1.519(16)
<P-O> Å)	1.531	1.531	1.530	1.532	1.532	1.533	1.534	1.533	1.533	1.534
Distt.	0.96×10^{-4}	0.89×10^{-4}	1.10×10^{-4}	0.86×10^{-4}	0.90×10^{-4}	0.82×10^{-4}	0.77×10^{-4}	1.08×10^{-4}	0.82×10^{-4}	1.00×10^{-4}

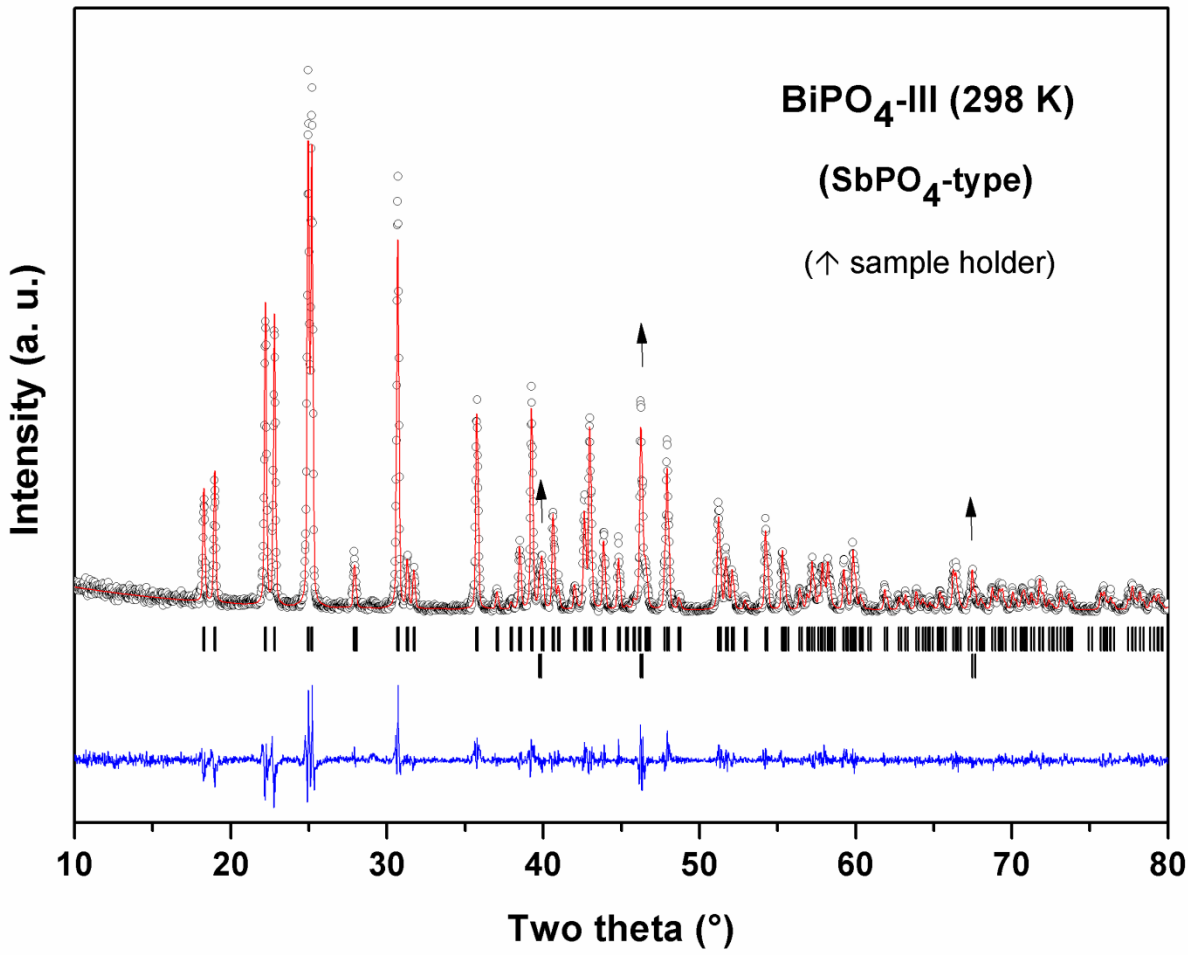

Fig.7. Rietveld refinement plot of the powder XRD data of $BiPO_4$-III at 298 K. (Only $SbPO_4$-type phases is observed). Arrows indicate reflections due to sample holder)

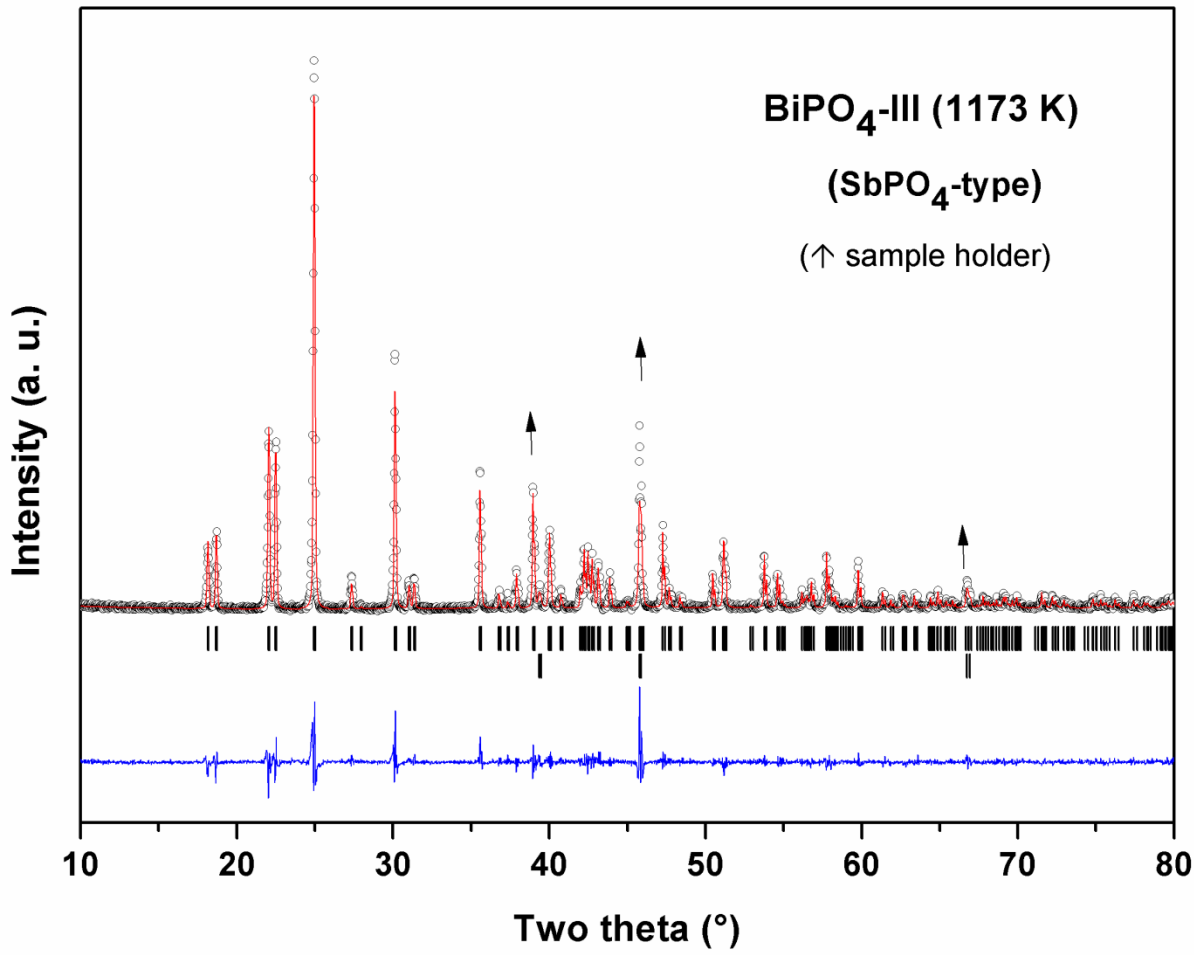

Fig.8. Rietveld refinement plot of the powder XRD data of $BiPO_4$-III at 1173 K. (Only $SbPO_4$-type phase is observed). Arrows indicate reflections due to sample holder)

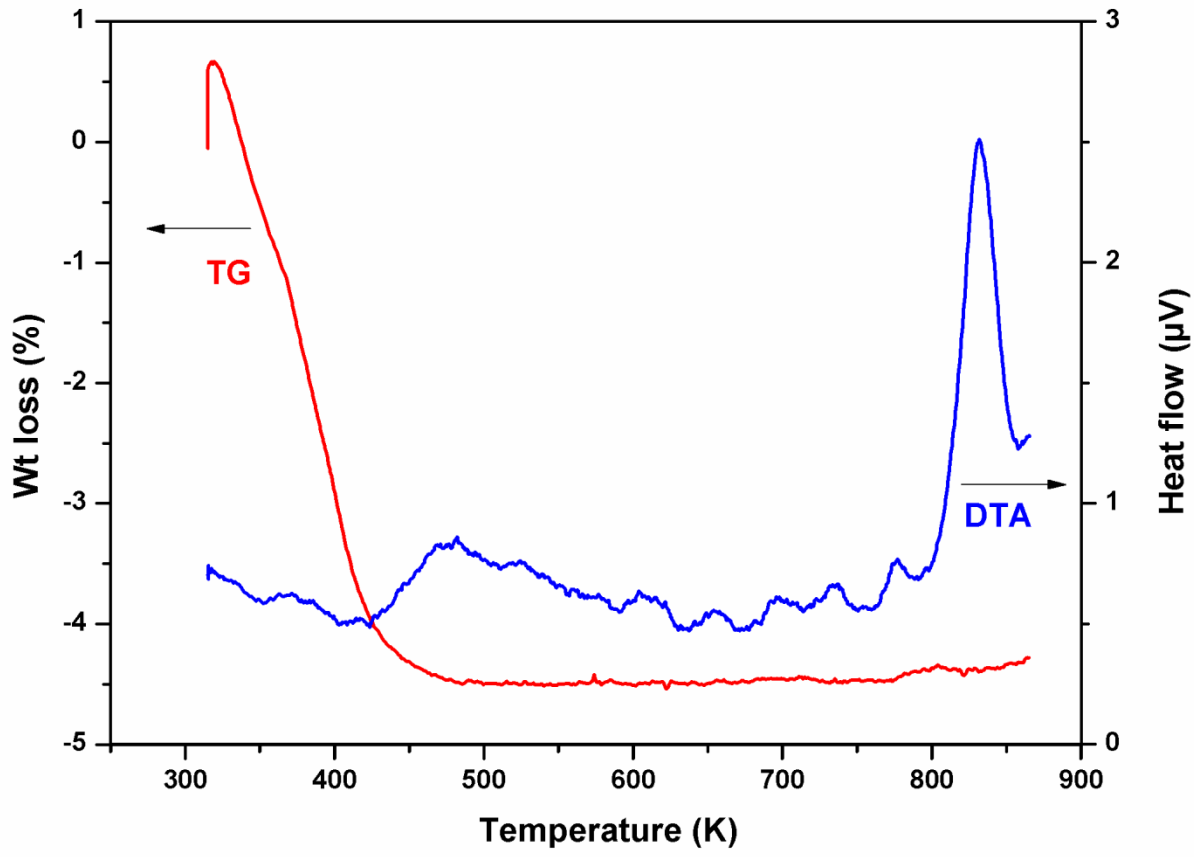

Fig.9. Typical TG-DTA traces of as prepared sample of hydrated trigonal $BiPO_4$ sample. (Sample was heated from 323 to 873 K at a rate of 10K/min).